SELECTED RESULTS FROM THE MARK II AT SPEAR[*]

Daniel L. Scharre
Stanford Linear Accelerator Center,
Stanford University, Stanford, Ca. 94305

ABSTRACT

Recent results on radiative transitions from the $\psi(3095)$, charmed meson decay, and the Cabibbo-suppressed decay $\tau \rightarrow K^* \nu_\tau$ are reviewed. The results come primarily from the Mark II experiment at SPEAR, but preliminary results from the Crystal Ball experiment on ψ radiative transitions are also discussed.

I. INTRODUCTION

This talk is the first of two reviewing recent results from SPEAR. I will concentrate on results from the Mark II experiment[1] and have selected three topics to discuss: radiative transitions from the $\psi(3095)$, charmed meson decays, and the Cabibbo-suppressed decay $\tau \rightarrow K^* \nu_\tau$. Some preliminary results from the Crystal Ball experiment[1] on ψ radiative transitions will also be presented.

The discussion on radiative transitions will be restricted to transitions from the ψ to ordinary hadrons, where ordinary hadrons are defined to be those which to first order do not contain charmed quarks. The status of the $\eta_c(2980)$ and radiative transitions to this state will be discussed in the next talk.[2] I will begin with a brief discussion of inclusive photon production at the ψ. This leads naturally into a discussion of the four exclusive radiative transitions which we (i.e., the Mark II) observe. Three of these transitions, to the η, $\eta'(958)$, and $f(1270)$, have been previously observed. Our results are in reasonable, but not perfect, agreement with the previous branching fraction measurements. The fourth observed transition is to a state which we tentatively identify as the E(1420). This transition has not been previously observed.

The discussion on charmed meson decays will cover new results on exclusive decay modes of the D and general inclusive properties of

the final states produced in D decays. Measurements of the mean charged particle multiplicity, the kaon fraction, and the electron fraction in D decays will be discussed. From the electron fractions, we have determined the inclusive D^o and D^+ semileptonic branching fractions, which allows a determination of the ratio of the D^o and D^+ total lifetimes.

Finally, we have measured the branching fraction for the Cabibbo-suppressed decay $\tau \rightarrow K^* \nu_\tau$. The measured branching fraction is consistent with expectations based on the previously measured, Cabibbo-favored decay $\tau \rightarrow \rho \nu_\tau$.

II. EXPERIMENTAL APPARATUS

The Mark II magnetic detector was designed to be a second-generation, general-purpose detector for doing physics at SPEAR (and a first-generation detector for doing physics at PEP). The design was based on the earlier SLAC-LBL magnetic detector[3] which was responsible for much of the pioneering work in e^+e^- annihilation physics done at SPEAR. The Mark II detector has significant advantages over the previous detector in its charged particle momentum resolution, time-of-flight resolution, neutral particle detection, lepton identification, and trigger design.

A schematic of the Mark II detector is shown in Fig. 1 viewed perpendicular to the beam direction. A particle traveling radially outwards from the interaction region passes through a 16-layer cylindrical drift chamber, a layer of scintillation counters which provide time-of-flight (TOF) information, a 1-radiation length aluminum coil (which provides a solenoidal field of approximately 4.2 kG in the central detector), a set of lead-liquid argon (LA) shower counter modules, and finally a set of proportional counters for muon identification. In addition to the muon counters which are shown above and below the detector in Fig. 1, there are additional muon proportional counter layers on both sides of the detector. Also, there are two additional shower counter modules (one LA module and one module consisting of two multi-wire proportional chamber planes) which cover the endcap regions.
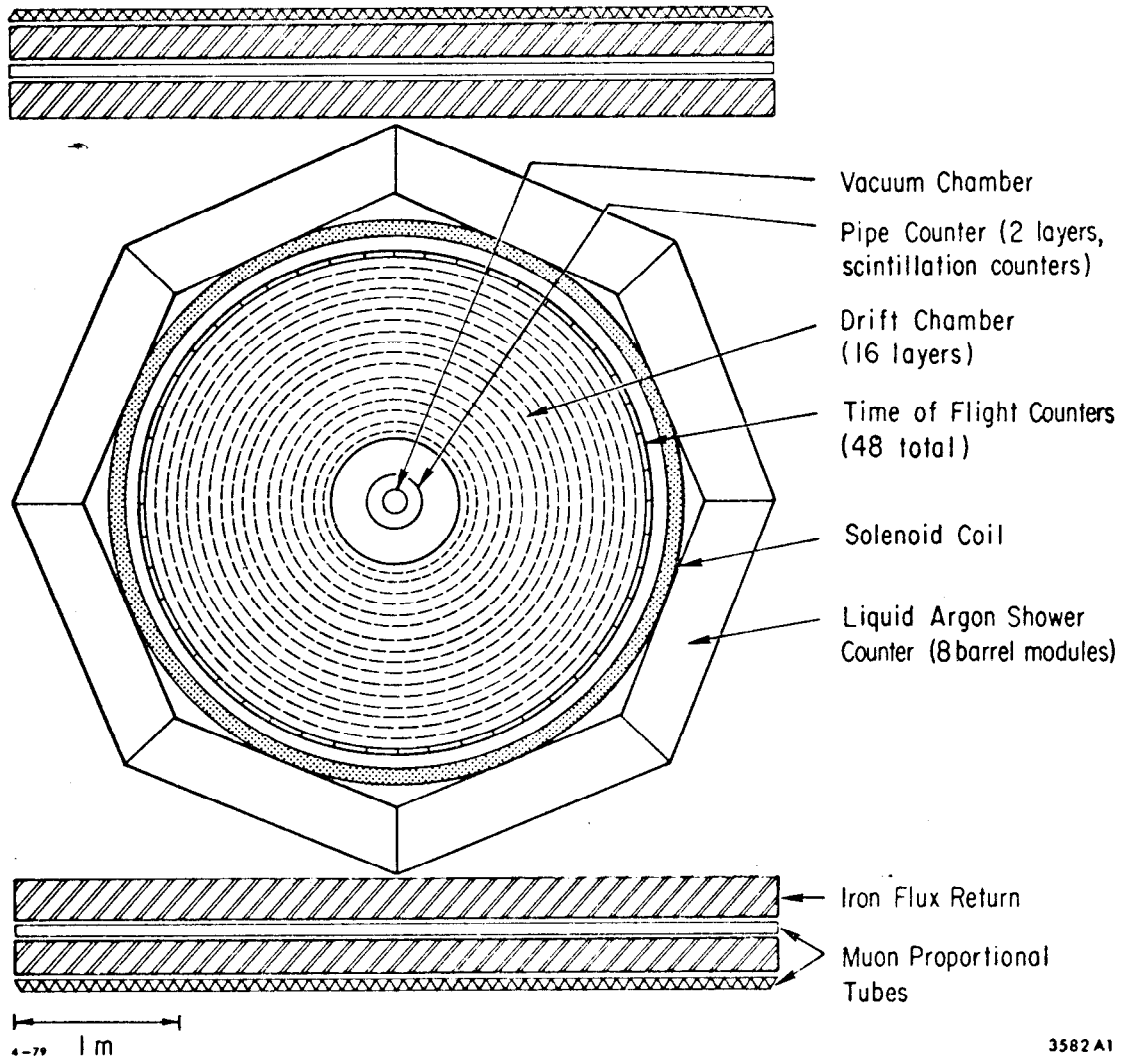
2

Fig. 1. Schematic of the Mark II magnetic detector viewed perpendicular to the beam direction. Not shown are the muon proportional counters on both sides of the detector and the endcap shower counters.

Charged tracks are reconstructed from hits in the 16 cylindrical drift chamber layers[4] of radii 0.37 m to 1.51 m which provide solid angle coverage over 85% of 4π sr. The azimuthal coordinates of charged tracks are measured to an rms accuracy of approximately 200 μm at each layer. The polar coordinates are determined from the 10 stereo layers oriented at $\pm3°$ to the beam axis. The momentum resolution can be expressed as $\delta p/p = [(0.0145)^2 + (0.005\ p)^2]^{\frac{1}{2}}$, where p is the momentum in GeV/c. The first term is the contribution from multiple Coulomb scattering and the second is the contribution

3

from the measurement error.[5] The tracking efficiency is greater than 95% for tracks with p > 100 MeV/c over 75% of 4π sr.

Photons are identified by energy deposits in the shower counter modules. The shower counter system[6] consists of eight LA barrel modules which surround the central detector and two endcap modules. The endcap modules have not been used extensively in the analysis, and I will restrict the remainder of the discussion to the barrel module system. Each module consists of approximately 14 radiation lengths of lead and argon, with readout strips parallel, perpendicular, and at 45° to the beam axis. The system of eight modules covers approximately 64% of 4π sr.

The rms energy resolution for electrons and photons detected in the LA has been determined from measurement of pulse height distributions from particles of known energy passing through the liquid argon. Figure 2 shows the ene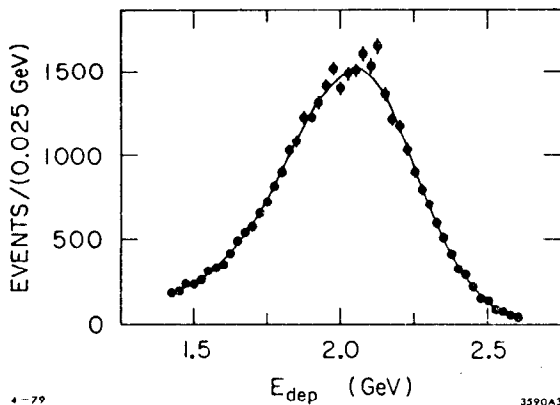rgy deposited in the LA for a sample of Bhabha events at 4.16 GeV center-of-mass energy ($E_{c.m.}$). The curve is a Gaussian resolution function, with $\delta E/E = 0.12\ E^{-\frac{1}{2}}$ (E in GeV), convoluted with the radiative tail. This expression provides a reasonable representation of the energy resolution for both electrons and photons of energies down to a few hundred MeV.

The rms angular resolution obtained for electromagnetic showers is typically 4 mrad, both in azimuth and dip angle, for high energy particles. At lower energies, the angular resolution can be a factor of two worse.

Fig. 2. Energy deposited in the LA for a sample of Bhabha events at $E_{c.m.}$ = 4.16 GeV. Curve is described in text.

Figure 3 shows the detection efficiency for γ's and π^{o}'s[7] in the LA as a function of energy. The measured values for the γ efficiency were obtained from 2-constraint (2C) fits to 2-prong and 4-prong events at the ψ according to the hypotheses $\psi \rightarrow \pi^{+}\pi^{-}\gamma(\gamma)$ and $\psi \rightarrow \pi^{+}\pi^{-}\pi^{+}\pi^{-}\gamma(\gamma)$,
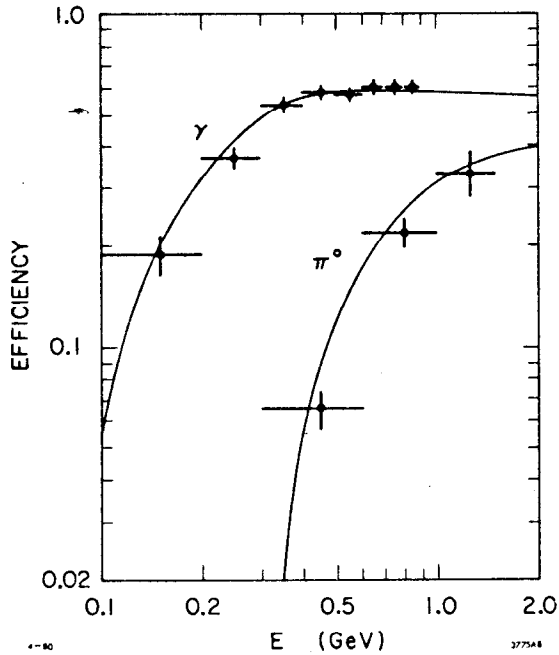
Fig. 3. Detection efficiency for
γ's and π^0's in the LA as a func-
tion of energy. Data points are
measured values and curves are
Monte Carlo estimates.

where a particle in parenthesis
is meant to imply an unobserved
particle. The π^0 mass constraint
was imposed on the $\gamma(\gamma)$ system.
The detection efficiency was cal-
culated from the fraction of
events in which the missing γ
was observed and tracked in the
LA. Corrections were made to
correct for the geometrical bias
imposed by the requirement that
all charged particles be observed
in the detector. A similar pro-
cedure was utilized to measure
the π^0 efficiency from 1C fits
according to the hypotheses
$\psi \rightarrow \pi^+\pi^-(\pi^0)$ and $\psi \rightarrow \pi^+\pi^-\pi^+\pi^-(\pi^0)$.
The π^0 detection efficiency was
calculated from the fraction of

events in which the missing π^0 was observed, with similar corrections
for geometrical bias. However, these π^0 efficiency measurements
must be considered as lower limits since the decays $\psi \rightarrow \pi^+\pi^-\gamma$ and
$\psi \rightarrow \pi^+\pi^-\pi^+\pi^-\gamma$ will successfully fit the corresponding hypothesis in
which the γ is replaced by a π^0, but no π^0 will be observed. The
solid curves represent the results of Monte Carlo determinations of
the γ and π^0 efficiencies employing the EGS electromagnetic shower
development code.[8]

Particle identification for hadrons is accomplished with 48 TOF
scintillation counters which surround the drift chamber and cover
approximately 75% of 4π sr. The rms time resolution is 0.30 ns for
hadrons. The average flight path of 1.85 m provides a separation of
pions from kaons up to momenta of 1.35 GeV/c and kaons from protons
up to 2.0 GeV/c at the 1-σ level.

Identification of electrons utilizes both the LA system and the
TOF system. For tracks with momenta less than 300 MeV/c, the electron

5

identification is based solely on TOF. For tracks with momenta greater
than 500 MeV/c, only the LA system is used for electron identifica-
tion. For tracks with momenta between 300 and 500 MeV/c, both TOF
and LA pulse height information is required for electron identifica-
tion. The hadron misidentification probability (i.e., the probability
that a hadron will be misidentified as an electron) is 7% for
$p < 500$ MeV/c, 4% for $p = 600$ MeV/c, and 2% for $p = 800$ MeV/c.

Muons are identified by hits in the muon proportional counter
system. This system consists of layers of proportional tubes (two
below and on each side of the detector and three above it) inter-
leaved with steel and covers approximately 55% of 4π sr. The
detection efficiency for muons within the solid angle of the detection
system with momenta greater than 700 MeV/c is greater than 98%. The
hadron misidentification probability is 4% for $p = 800$ MeV/c, 11%
for $p = 900$ MeV/c and 2% for $p > 1$ GeV/c.

The detector is triggered with a two-stage hardware trigger,[9]
selecting (with efficiency greater than 99%) all interactions emitting
two or more charged tracks, each with transverse momentum greater
than 100 MeV/c, within the solid angle covered by the drift chamber,
one of which must be within the central region of the drift chamber
which covers 67% of 4π sr. The luminosity is measured with indepen-
dent shower counters detecting Bhabha scattering at 22 mrad, and
checked against wide-angle Bhabha events observed in the central
detector.

It is customary in a talk such as this to show a computer
reconstruction of a "typical" event to impress other experimenters
with how well the detector works. Figure 4 shows a resconstruction
of an event corresponding to the $\psi'(3684)$ decay[10]

$$\psi' \to \pi^+\pi^-\psi \quad , \quad \psi \to \mu^+\mu^- \quad .$$

One can see that there is no problem tracking the charged particles
through the drift chamber. The flight time of each track is deter-
mined by a TOF counter (represented by a rectangle at the end of each
reconstructed drift chamber track). Finally, unambiguous identifica-
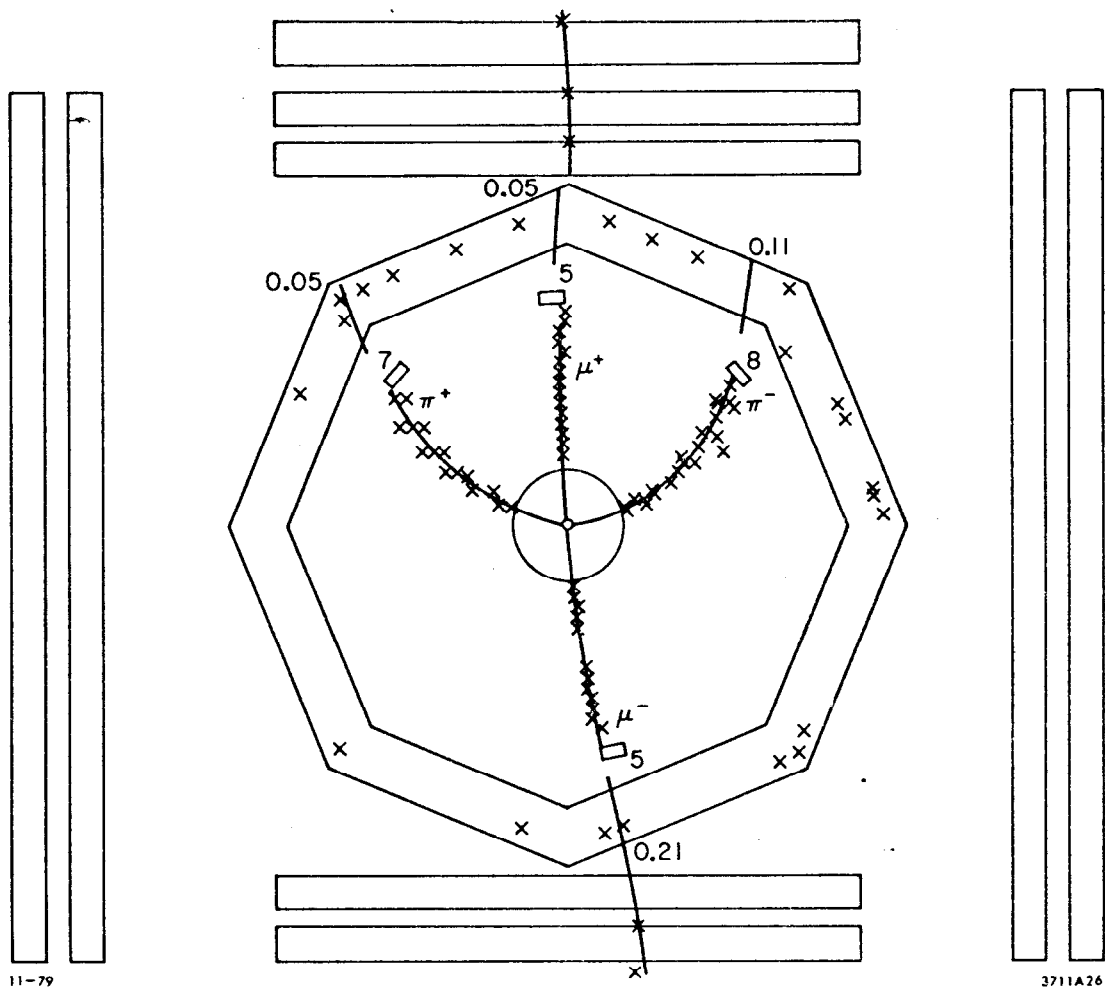tions of the muons are made in the muon proportional counter system.

Fig. 4. Computer reconstruction of typical event in the Mark II detector.

As the tracks are all due to the minimum-ionizing particles, no large energy deposits are observed in the LA.

III.   RADIATIVE TRANSITIONS FROM THE $\psi(3095)$

Measurements of inclusive photon production at the $\psi(3095)$ by this experiment[11] and the Lead-Glass Wall (LGW) experiment[12] have shown that there is a sizable direct photon component in the momentum spectrum. However, because of the relatively poor photon energy resolutions of our LA shower counter system and the lead-glass counters in the LGW ($\delta E/E \approx 9\%/E^{1/2}$, E in GeV), neither experiment was able to observe any narrow structure in the inclusive photon momentum distribution.

7

The Crystal Ball detector[13] was designed to provide good energy resolution for electromagnetic showers. The use of NaI(Tℓ) for shower detection presently allows a resolution of $\delta E/E \approx 2.8/E^{1/4}$ (E in GeV) to be obtained.

Figure 5 shows a preliminary measurement of the inclusive γ energy distribution of the ψ from the Crystal Ball.[14] It is plotted as a function of the logarithm of the γ energy (E_γ in MeV) so that the bin width is roughly proportional to the energy resolution at all energies. This distribution is based on a sample of approximately 900,000 events obtained during approximately two weeks of running near the peak of the ψ. Details of the analysis can be found in Ref. 13.

The structure observed in Fig. 5 is evidence for exclusive processes of the type
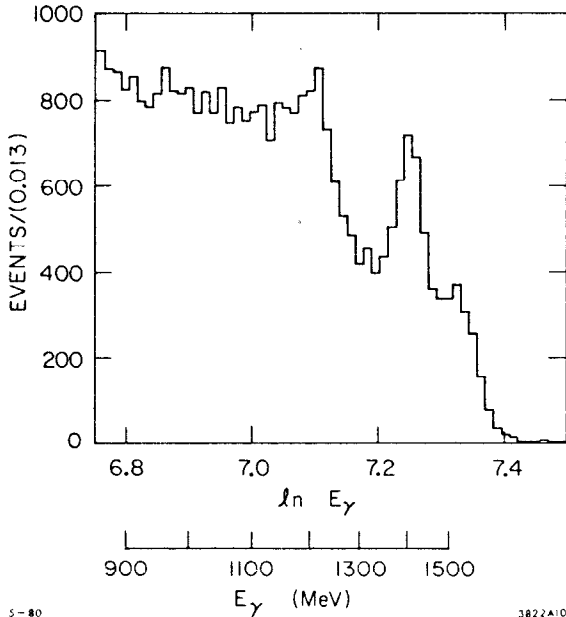
$$\psi \to \gamma + X \ .$$

Fig. 5. Inclusive γ distribution at the ψ as a function of the logarithm of the γ energy in MeV (data from the Crystal Ball collaboration).

There is clear evidence for the radiative transitions to the η,[15-17] $\eta'(958)$,[15-18] and a new state which I will refer to as the E(1420) which has recently been observed by us.[19] [Although I refer to this state as the E(1420), this assignment is still open to question.] An additional transition which has been previously observed is $\psi \to \gamma$ f(1270).[20,21] Because of the relatively small branching fraction for this transition, it is not observed in this inclusive distribution. Each of these four transitions will be discussed in turn in the following sections.

A. $\psi \to \gamma\eta, \ \gamma\eta'$

As the η and η' are members of the same SU(3) nonet, it makes sense to discuss the radiative transitions to these two states at the

8

same time, along with the transition to the π^0. I will take the extremely naive approach that it is possible to understand these pro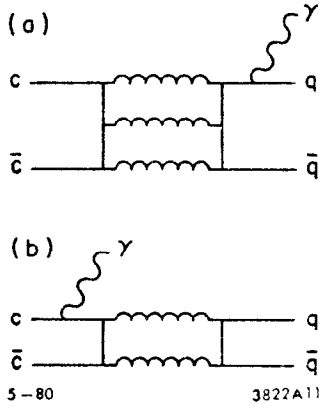cesses in terms of leading-order QCD diagrams. Thus, one can imagine that the radiated photon is produced either from the outgoing quark line (assumed to be u, d, or s) as in Fig. 6(a) or from the initial charmed quark line as in Fig. 6(b). In the first case, the minimal coupling between the charmed quark line and the ordinary quark line requires three gluons. In the second case, two gluons are sufficient.

Fig. 6. Leading-order diagrams for radiative transitions from the ψ with a) photon emission from the final-state quark line and b) photon emission from the initial-state charmed quark line.

Let me first consider only the process shown in Fig. 6(a) and assume it is the dominant one. By invoking vector-meson dominance, I can relate the $\gamma\pi^0$ and $\rho^0\pi^0$ decay widths

$$\Gamma(\psi \to \gamma\pi^0) = (\alpha\pi/\gamma_\rho^2)\Gamma(\psi \to \rho^0\pi^0) \quad .$$

This leads to a prediction for the $\gamma\pi^0$ branching fraction $B(\psi \to \gamma\pi^0) \approx 2 \times 10^{-5}$ from the measured $\rho^0\pi^0$ branching fraction.[18,22,23] This is consistent with the experimental measurement[16] $B(\psi \to \gamma\pi^0) = (7 \pm 5) \times 10^{-5}$.

The next step is to relate the widths of the $\gamma\eta$ and $\gamma\eta'$ transitions to the width of the $\gamma\pi^0$ transition. The η and η' have the following SU(3) singlet and octet components

$$\eta = \eta_8 \cos\theta + \eta_1 \sin\theta$$

$$\eta' = -\eta_8 \sin\theta + \eta_1 \cos\theta \quad ,$$

where θ is the standard octet-singlet mixing angle. If one assumes SU(3) invariance, only the octet components contribute to the process shown in Fig. 6(a) and one obtains (up to phase space corrections)

$$\Gamma(\psi \to \gamma\pi^0):\Gamma(\psi \to \gamma\eta):\Gamma(\psi \to \gamma\eta') = 3:\cos^2\theta:\sin^2\theta \quad .$$

Using the experimentally determined mixing angle $\theta = -11°$, one calculates

$$\Gamma(\psi \to \gamma\pi^o):\Gamma(\psi \to \gamma\eta):\Gamma(\psi \to \gamma\eta') = 3:0.96:0.04 \quad,$$

which grossly contradicts the experimental measurements.[15-18] The $\gamma\eta'$ branching fraction has been experimentally determined to be larger than the $\gamma\eta$ branching fraction, and both are at least an order of magnitude larger than the π^o transition. The conclusion is that the process in Fig. 6(b) is the dominant one.

One can proceed with similar calculations for the second process [shown in Fig. 6(b)]. Assuming SU(3) invariance (now only the singlet components contribute) and ignoring phase space corrections, one obtains

$$\Gamma(\psi \to \gamma\pi^o):\Gamma(\psi \to \gamma\eta):\Gamma(\psi \to \gamma\eta') = 0:\sin^2\theta:\cos^2\theta \quad.$$

This is qualitatively in better agreement with the data. However, the predicted ratio $\Gamma(\psi \to \gamma\eta')/\Gamma(\psi \to \gamma\eta)$ is much larger than the experimentally measured ratio.

If one allows for SU(3) symmetry breaking, these results are modified. Fritzsch and Jackson[24] have calculated the relative widths of the $\gamma\eta$ and $\gamma\eta'$ transitions by considering gluon-mediated mixing between the three isoscalar states η, η', and $\eta_c(2980)$. Based on the experimental masses of these states, they find the following admixture of η and η' in the η_c:

$$\eta_c = c\bar{c} + \varepsilon\cdot\eta + \varepsilon'\cdot\eta' \quad,$$

where $\varepsilon \approx 10^{-2}$ and $\varepsilon' \approx 2.2 \times 10^{-2}$. The decay widths (for M1 transitions) for $\gamma\eta$ and $\gamma\eta'$ are

$$\Gamma(\psi \to \gamma\eta) = \varepsilon^2 \frac{4\alpha}{3m_c^2} \left(\frac{2}{3}\right)^2 k^3 \Omega^2$$

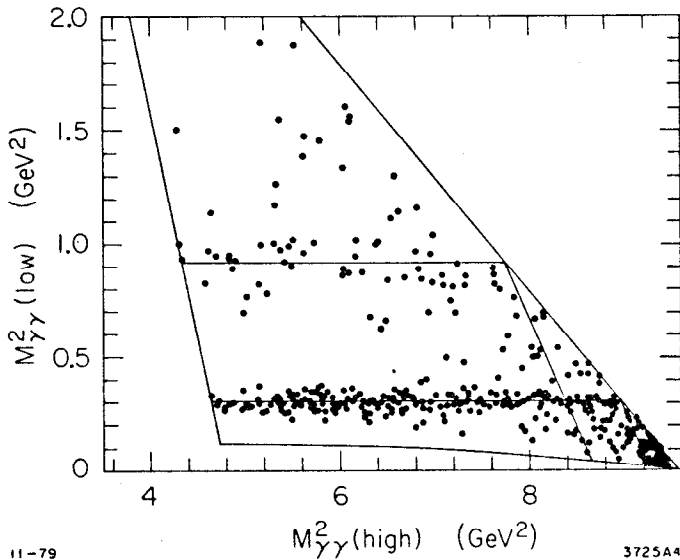$$\Gamma(\psi \to \gamma\eta') = (\varepsilon')^2 \frac{4\alpha}{3m_c^2} \left(\frac{2}{3}\right)^2 (k')^3 \Omega^2 \quad,$$

where m_c is the charmed quark mass, $k(k')$ is the momentum of the $\eta(\eta')$, and Ω is an overlap integral. If it is assumed that the overlap integral is the same for both the η and η' transitions, one finds for the ratio of the two partial widths

10

$$\frac{\Gamma(\psi \to \gamma\eta')}{\Gamma(\psi \to \gamma\eta)} = \left(\frac{k'}{k}\right)^3 \left(\frac{\epsilon'}{\epsilon}\right)^2 \approx 3.9 \quad .$$

By estimating the overlap integral $\Omega^2 \approx 0.1$, Fritzsch and Jackson also make predictions for the absolute values of the widths, $\Gamma(\psi \to \gamma\eta) \approx 60$ eV and $\Gamma(\psi \to \gamma\eta') \approx 220$ eV.

Branching fractions for the transitions $\psi \to \gamma\eta$ and $\psi \to \gamma\eta'$ have recently been published by the Crystal Ball collaboration.[17] The measurements were based on a sample of decays $\psi \to 3\gamma$. Figure 7 shows the Dalitz plot for this sample of events. Two distinct bands associated with $\gamma\eta$ and $\gamma\eta'$ transitions are observed.[25] The branching fractions for these transitions were determined from a fit to the Dalitz plot. They are

$B(\psi \to \gamma\eta') =$ $(6.9 \pm 1.7) \times 10^{-3}$ and $B(\psi \to \gamma\eta) =$ $(1.2 \pm 0.2) \times 10^{-3}$.

Fig. 7. Dalitz plot for $\psi \to 3\gamma$. Boundary includes effects of both kinematics and $\gamma\gamma$ opening angle cuts (data from the Crystal Ball collaboration).

We have measured the branching fraction for the process[26]

$$\psi \to \gamma\eta' \ , \ \eta' \to \pi^+\pi^-\gamma \quad .$$

The data sample used in this analysis is basically the same as the Crystal Ball data sample, as both experiments were running at SPEAR simultaneously.[27] Events with two oppositely charged tracks identified as pions and two or more photons[28] observed in the LA shower counter modules were fit to the hypothesis

$$\psi \to \pi^+\pi^-\gamma\gamma \quad . \tag{1}$$

Events in which the fitted $\gamma\gamma$ invariant mass was between 0.12 and 0.15 GeV (i.e., consistent with the π^0 mass) were eliminated. The $\pi^+\pi^-\gamma$ invariant mass distribution for the events which remained after

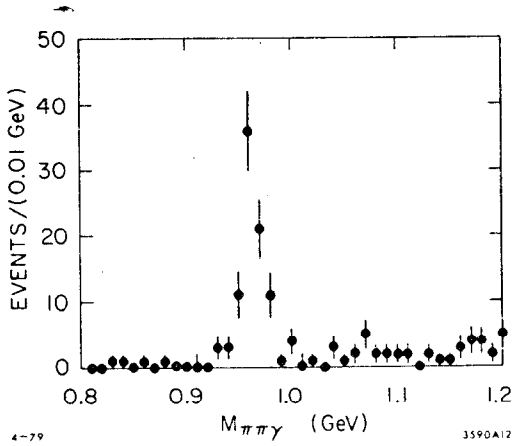the χ^2 and π^0 cuts is shown in Fig. 8. From Monte Carlo calculations of the detection efficiency (which included an assumed $1 + \cos^2\theta$ dependence for the ψ decay, where θ is the angle between the photon and the beam direction), we measured the branching fraction $B(\psi \to \gamma\eta') = (3.4 \pm 0.7) \times 10^{-3}$.

Due to the bias imposed by the trigger requirement,[29] we are unable to observe the reaction

$$e^+e^- \to \psi \to 3\gamma \quad .$$

In order to measure the $\gamma\eta$ branching fraction, it was necessary to analyze the more complicated process[30]

$$\psi' \to \pi^+\pi^-\psi \; , \; \psi \to 3\gamma \quad . \qquad (2)$$

Fig. 8. $\pi^+\pi^-\gamma$ invariant mass distribution for events satisfying (1) with π^0 combinations eliminated.

The $\pi^+\pi^-$ from the ψ' cascade decay provided the trigger. Figure 9 shows the invariant mass of the low-mass $\gamma\gamma$ combinations for the 10 events satisfying fits to (2). Eight are peaked at the η mass. From this, the branching fraction $B(\psi \to \gamma\eta) = (0.9 \pm 0.4) \times 10^{-3}$ is obtained.

In Table I is a compilation of our results and the Crystal Ball results, along with the previous experimental results, for the $\gamma\eta$ and $\gamma\eta'$ branching fractions. Our measurement of the $\gamma\eta'$ branching fraction is somewhat larger than, but still consistent with, the previous measurements. The Crystal Ball finds a branching fraction that

Fig. 9. Low-mass $\gamma\gamma$ invariant mass combinations for events satisfying (2).

Table I. Branching fractions for radiative transitions
from the ψ to the η and η'.

decay	mode	branching fraction	experiment
$\psi \to \gamma\eta'$	$\rho^0\gamma$	$(3.4 \pm 0.7) \times 10^{-3}$	Mark II
	$\gamma\gamma$	$(6.9 \pm 1.7) \times 10^{-3}$	Crystal Ball
	$\gamma\gamma$	$(2.2 \pm 1.7) \times 10^{-3}$	DASP[a]
	$\rho^0\gamma$	$(2.4 \pm 0.7) \times 10^{-3}$	DESY-Heidelberg[b]
		3.3×10^{-3}	theory[c]
$\psi \to \gamma\eta$	$\gamma\gamma$	$(0.9 \pm 0.4) \times 10^{-3}$	Mark II
	$\gamma\gamma$	$(1.2 \pm 0.2) \times 10^{-3}$	Crystal Ball
	$\gamma\gamma$	$(0.8 \pm 0.2) \times 10^{-3}$	DASP[a]
	$\gamma\gamma$	$(1.3 \pm 0.4) \times 10^{-3}$	DESY-Heidelberg[b]
		0.9×10^{-3}	theory[c]

[a] Ref. 16

[b] Refs. 15, 18

[c] Ref. 24

is twice as large as ours. This discrepancy is not totally understood.
However, it should be noted that the two measurements are based on
different decay modes of the η', and at least part of the discrepancy
may come from the uncertainty in the relative branching fractions of
the two decay modes. On the other hand, all four determinations of
the branching fraction to $\gamma\eta$ are consistent. Also shown in Table I
are the theoretical predictions calculated by Fritzsch and Jackson.[24]
The excellent agreement between theory and experiment is better than
one has a right to expect because of the uncertainties in the calcu-
lations.

Table II summarizes the measurements of the ratio
$B(\psi \to \gamma\eta')/B(\psi \to \gamma\eta)$. The measured values range from approximately
2 to 6 and the theoretical prediction is 3.9. Thus, I think it is
fair to say that we have a reasonable understanding of the M1 transi-
tions from the ψ to the ordinary pseudoscalar meson states.

In order to further explore the properties of the charmonium
system, the Crystal Ball and Mark II collaborations have begun similar

Table II. $B(\psi \to \gamma\eta')/B(\psi \to \gamma\eta)$.

ratio	experiment
3.8 ± 1.9	Mark II
5.9 ± 1.5	Crystal Ball
2.8 ± 2.3	DASP[a]
1.8 ± 0.8	DESY-Heidelberg[b]
3.9	theory[c]

[a] Ref. 16

[b] Refs. 15, 18

[c] Ref. 24

studies of radiative transitions from the ψ'. Naively, one would expect these branching fractions to be approximately an order of magnitude smaller than the corresponding branching fractions at the ψ.[31] Presently, no evidence for $\gamma\eta$ or $\gamma\eta'$ production from the ψ' has been observed, with preliminary 90% confidence level upper limits from the Crystal Ball of $B(\psi' \to \gamma\eta') < 8 \times 10^{-4}$ and $B(\psi' \to \gamma\eta) < 10^{-4}$. As these limits are only a factor of eight below the measured ψ branching fractions, there is no reason to worry about the absence of these signals at this time.

B. $\psi \to \gamma f(1270)$

In order to understand the radiative transition to the f(1270), I will once more consider the two processes shown in Fig. 6. The measured branching fraction for the process $\psi \to \omega f$ is approximately 3×10^{-3}.[32] Invoking VMD for the process shown in Fig. 6(a), one is led to expect a rate for the γf transition which is considerably less than the measured value.[20,21] Thus, even in this case, where the final state has $J^P = 2^+$ rather than 0^-, it appears that the process in Fig 6(b) is dominant.

We have measured the branching fraction for the γf transition.[33] Figure 10 shows the $\pi^+\pi^-$ invariant mass distribution (data points with error bars) for events which satisfy a fit to the hypothesis

$$\psi \to \pi^+\pi^-\gamma \tag{3}$$

with $\chi^2 < 15$. Two structures are evident in the mass distribution, one at the ρ mass and the other at the f(1270) mass. Since the decay $\psi \to \rho^0\gamma$ does not conserve charge conjugation parity (C-parity), it is assumed that the events in the ρ^0 mass region resulted from $\rho^0\pi^0$ decays in which an asymmetric decay of the π^0 led to an acceptable fit to (3). A Monte Carlo was used to determine the $\pi^+\pi^-\pi^0$ feeddown
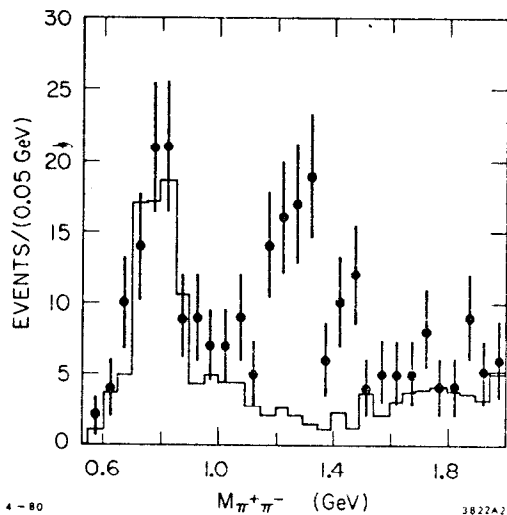
14

Fig. 10. $\pi^+\pi^-$ invariant mass distribution for events satisfying (3). Histogram shows the expected feeddown from the $\pi^+\pi^-\pi^0$ final state as determined by Monte Carlo.
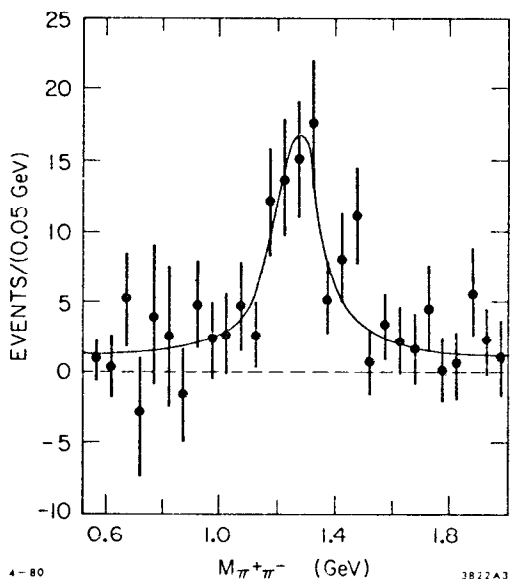

Fig. 11. $\pi^+\pi^-$ invariant mass distribution after subtraction of $\pi^+\pi^-\pi^0$ feeddown. Curve is described in text.

into the $\pi^+\pi^-\gamma$ channel. The resulting distribution (including production of both $\rho^0\pi^0$ and $\rho^{\pm}\pi^{\mp}$) is compared with the data in Fig. 10 and can clearly account for the observed ρ^0 peak.

Figure 11 shows the $\pi^+\pi^-$ mass distribution after subtraction of the $\pi^+\pi^-\pi^0$ background. The distribution is dominated by the f. An expression consisting of a Breit-Wigner resonance term plus a flat background term was fitted to this distribution. The curve in Fig. 11 shows the best fit which gave M = 1280 MeV and Γ = 180 MeV for the resonance parameters. The branching fraction for (3) was found to be $B(\psi \to \gamma f) = (1.3 \pm 0.3) \times 10^{-3}$. This branching fraction is consistent with the previously measured values of $B(\psi \to \gamma f) = (2.0 \pm 0.3) \times 10^{-3}$ from PLUTO[20] and $B(\psi \to \gamma f)$ between $(0.9 \pm 0.3) \times 10^{-3}$ and $(1.5 \pm 0.4) \times 10^{-3}$ (depending on the helicity of the f in the final state) from DASP.[21]

As pointed out in the previous section, we seem to have a fairly good understanding of the transitions to the I_z = 0 members of the $J^P = 0^-$ nonet. If measurements of the radiative transitions

15

to the f' and A_2^o could be made, we would have an additional check on the theoretical ideas discussed previously. We have preliminary results which show no evidence for transitions to either of these two states. They give 90% confidence level upper limits of $B(\psi \to \gamma f') \times B(f' \to K\bar{K}) < 10^{-3}$ and $B(\psi \to \gamma A_2^o) < 10^{-3}$. Unfortunately, these limits are not yet small enough to provide meaningful constraints on models. As in the case of the $\gamma\pi^o$ transition, one expects to see a very small branching fraction for γA_2^o because of isospin conservation. However, the $\gamma f'$ transition should be observable. Based on a naive calculation assuming SU(3) invariance (similar to the η-η' calculation described earlier,[34] one expects

$$\frac{B(\psi \to \gamma f')}{B(\psi \to \gamma f)} = \frac{1}{2} \quad .$$

Our limit is not yet inconsistent with this prediction.

C. $\psi \to \gamma E(1420)$

As the E(1420) is a fairly obscure resonance, I will briefly review what was known about the E as of the last (1978) Particle Data Group tables[35] before discussing the results on the γE radiative transition. The E is a fairly narrow resonance with width estimates ranging from 40 to 80 MeV. Measurements of the mass lie between 1400 and 1440 MeV. None of the quantum numbers of the E have been firmly established. The isospin is believed to be zero as no charged E has ever been observed; the C-parity is believed to be even; and analyses of the decay Dalitz plot favor an abnormal spin-parity assignment. $J^P = 0^-$ and 1^+ are the preferred values. The principally observed decay mode is $K\bar{K}\pi$, but there is some evidence for an $\eta\pi\pi$ decay mode. Finally, up until 1978, the best signals for the E were observed in $\bar{p}p$ annihilations at rest. I will mention only one of these experiments here. Baillon et al.[36] studied a sample of $\bar{p}p$ annihilations in the CERN 81-cm hydrogen bubble chamber. They did a spin-parity analysis of the E observed in the reaction $\bar{p}p \to E\pi\pi$ and determined $J^P = 0^-$.

We see evidence for the process[19]

$$\psi \to \gamma E \, , \, E \to K_S K^{\pm} \pi^{\mp} \quad . \tag{4}$$

16

Observation of this transition establishes C = + for the E.

Figure 12(a) shows the $K_S K^{\pm} \pi^{\mp}$ invariant mass for events satisfying the 5C fit to (4) with $\chi^2 < 15$.[37] The constraints are the normal ones of energy-momentum conservation with an additional constraint for the K_S mass. A peak is seen near the mass of the E(1420). One is not compelled to interpret this structure as the E(1420), but due to the similar characteristics of this structure and the previously observed E, I will make this tentative assignment.

The parameters of the resonance were obtained by fitting the invariant mass distribution to a Breit-Wigner[38] plus a smooth background. We find $M = 1.44^{+0.01}_{-0.015}$ GeV and $\Gamma = 0.05^{+0.03}_{-0.02}$ GeV. These errors include systematic uncertainties due to the functional form used in the fit. The branching fraction product, based on
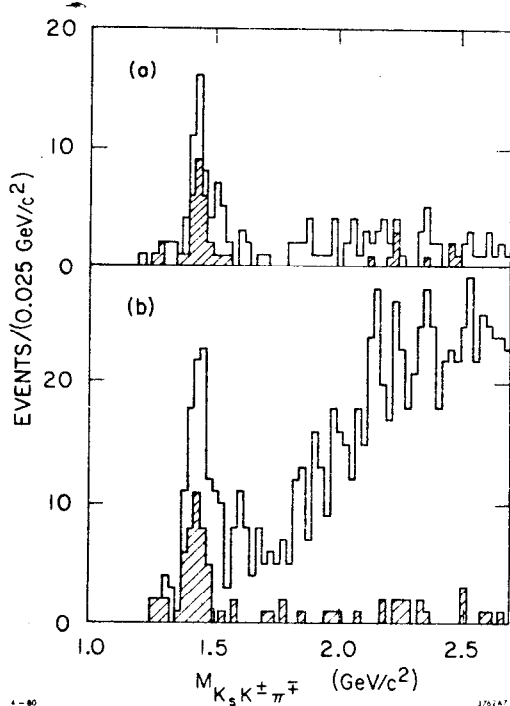

Fig. 12. $K_S K^{\pm} \pi^{\mp}$ invariant mass distributions for events satisfying a) 5C fits and b) 2C fits (i.e., observation of the photon is not required) to (4). Shaded regions have the additional requirement $M_{K\bar{K}} < 1.05$ GeV.

47 ± 12 observed events, is $B(\psi \to \gamma E) \times B(E \to K_S K^{\pm} \pi^{\mp}) =$ $(1.2 \pm 0.5) \times 10^{-3}$.[39] With the assumptions that the E is an isoscalar and that K_S and K_L production are equal in the decay of the E, one can relate the $K^+ K^- \pi^0$, $K^0 \bar{K}^0 \pi^0$, and $K^0 K^{\pm} \pi^{\mp}$ branching fractions and determine the branching fraction product

$B(\psi \to \gamma E) \times B(E \to K\bar{K}\pi) = (3.6 \pm 1.4) \times 10^{-3}$.

Previous experiments[35] have found the decay of the E to be associated with a low mass $K\bar{K}$ enhancement which we also observe. If a cut requiring $M_{K\bar{K}} < 1.05$ GeV is imposed on the data, the shaded region in Fig. 12(a) is obtained.

17

Since the signal is quite clean, it is possible to relax the requirement that the photon be observed. The resulting 2C fit to (4) is shown in Fig. 12(b). Although there is an improvement in statistics,[40] there is also an increase in the background level. However, as shown by the shaded region, the $K\overline{K}$ mass cut again substantially reduces the background.

The Dalitz plot for the sample of events shown in Fig. 12(b) with masses between 1.375 and 1.500 GeV (the signal region) is shown in Fig. 13. The curves show t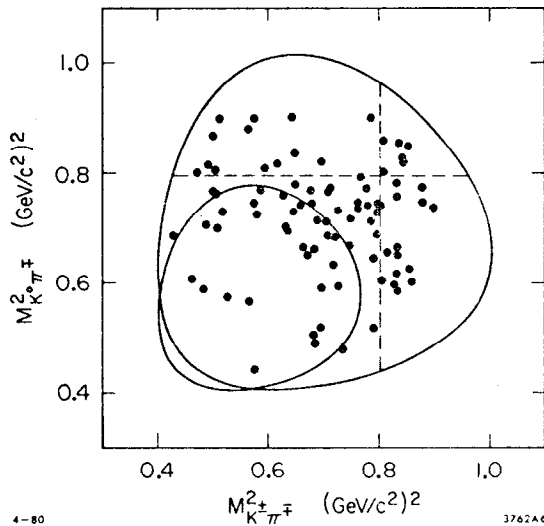he low-mass and high-mass kinematic boundaries and the dashed lines show the nominal $K^*(890)$ mass values. The points are plotted as functions of the $(K\pi)^o$ invariant mass squared vs. the $(K\pi)^{\pm}$ invariant mass squared. The $K\overline{K}$ axis, if it were shown, would be at an angle approximately bisecting the two $K\pi$ axes. One sees an excess of events in the upper right-hand corner of the Dalitz plot.[41] It is not clear whether these events correspond to a low-mass $K\overline{K}$ enhancement (spread out by the movement of the kinematic boundary as the $K\overline{K}\pi$ mass changes), or to constructive interference where the K^* bands overlap.

Fig. 13. Dalitz plot for events with $1.375 \leq M_{K\overline{K}\pi} < 1.500$ GeV. Curves show low-mass and high-mass kinematic boundaries. Dashed lines show nominal K^* mass values.

Figure 14(a) shows the $K_S K^{\pm}$ invariant mass distribution for events in the signal region and Fig. 14(b) shows the corresponding distribution for events outside the signal region. There is evidence for a low-mass $K\overline{K}$ enhancement for events in the signal region which is absent for events outside the signal region. One possible interpretation of this enhancement is the $\delta(980)$.
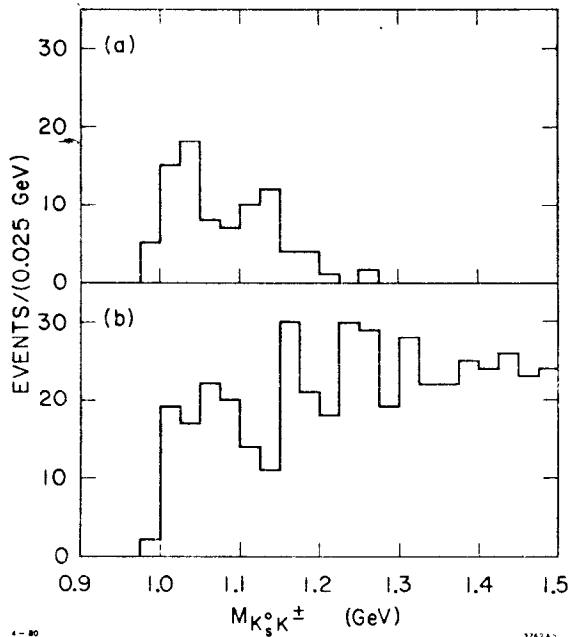
Fig. 14. $K_S K^{\pm}$ invariant mass distributions for events a) in the signal region and b) outside the signal region.

In an attempt to understand the decay mechanism of the E, fits were made to the Dalitz plot which included $K^* \overline{K}$ (the inclusion of both this state and the charge conjugate state are implied by this notation), $\delta\pi$, and phase space contributions. These three contributions were added incoherently, but the $K^* \overline{K}$ contribution included components from both the charged and neutral K^* states, which were assumed to interfere constructively where they cross on the Dalitz plot (as demanded by the even C-parity of the E). The best fit favors $\delta\pi$ as the primary component of the decay with

$$\frac{B(E \to \delta\pi) \times B(\delta \to \overline{KK})}{B(E \to \overline{KK}\pi)} = 0.8 \pm 0.2$$

The quoted error does not include possible systematic errors. One has to be careful in interpreting this result, as the best fit to the Dalitz plot does not completely simulate the $\overline{KK}$ invariant mass distribution. This indicates that the decay mechanism is not completely understood.

An attempt has been made to determine the spin of the E by analysis of the double decay angular distribution for events consistent with

$$\psi \to \gamma E \ , \ E \to \delta\pi \quad .$$

However, the limited statistics do not allow a statistically significant determination of the spin.

Preliminary results from the Crystal Ball also show evidence for the transition $\psi \to \gamma E$.[14] Figure 15 shows the $K^+K^-\pi^0$ invariant mass distribution[42] for events which satisfy the 2C fit to

$$\psi \to \gamma K^+ K^- \pi^0 \quad , \qquad (5)$$

with $M_{K\bar{K}} < 1.1$ GeV. Although the Crystal Ball detector has excellent energy resolution for photons, the absence of a magnetic field does not allow a momentum measurement for charged particles. This reduces the constraint class for (5) from 4 to 2. Evidence for an E signal is seen in this distribution. As the Crystal Ball efficiency calculations are still in a very preliminary state, estimates of the branch-
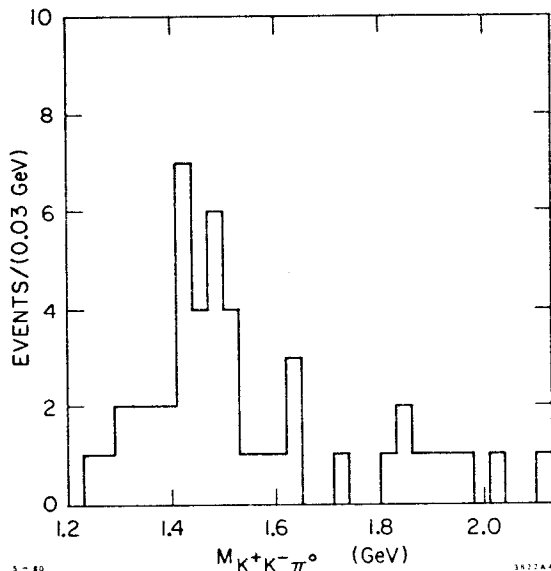

Fig. 15. $K^+K^-\pi^0$ invariant mass distribution for events satisfying (5) with $M_{K\bar{K}} < 1.1$ GeV (data from the Crystal Ball collaboration).

ing fraction are only good to a factor of two at best. When correc-tions are made for the K^+K^- mass cut[43] and the unobserved decay modes of the E, they find $B(\psi \to \gamma E) \times B(E \to K\bar{K}\pi) \approx 2 \times 10^{-3}$.

As was mentioned earlier, there is some evidence for the decay of the E into $\eta\pi^+\pi^-$. Figure 16 shows the $\eta\pi^+\pi^-$ invariant mass dis-tribution (from the Crystal Ball) for events satisfying fits to

$$\psi \to \gamma\eta\pi^+\pi^- \quad . \qquad (6)$$

In addition to the η' signal, there is evidence for a peak in the E mass region. A preliminary estimate of the branching fraction product $B(\psi \to \gamma E) \times B(E \to \eta\pi\pi)$ finds it to be smaller than the corresponding number for $K\bar{K}\pi$, but a firm number will have to wait until calculations of the efficiencies are made.

To summarize our results, the E is observed very strongly in radiative transitions from the ψ. The only other transition that has
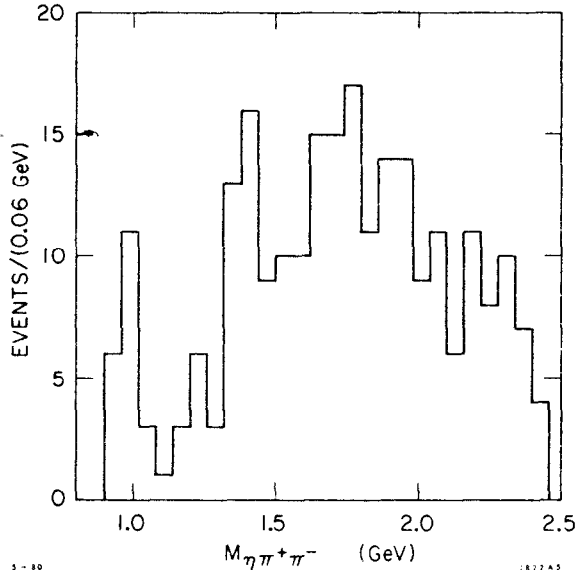
Fig. 16. $\eta\pi^+\pi^-$ invariant mass distribution for events satisfying (6) (data from the Crystal Ball collaboration).

been observed with a comparable branching fraction is the $\gamma\eta'$ transition. Observation of this transition has established the C-parity of the E as even. Unfortunately, a determination of the spin is impossible with the present statistics. Finally, we find the $\overline{KK}\pi$ decay mode of the E to be predominantly $\delta\pi$.

Recent results on the E have come from two hadronic experiments which I would like to discuss briefly, as these results are relevant to the interpretation of the E. The first results are from a high statistics (90 events/μb) bubble chamber experiment in which the reaction

$$\pi^- p \to K_S K^\pm \pi^\mp n$$
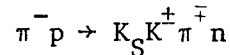
was studied at 3.95 GeV/c.[44] They observe significant E production, and measure values for the E mass and width of M = 1426 ± 6 MeV and Γ = 40 ± 15 MeV. A partial-wave analysis of the data determined the spin-parity of the E to be $J^P = 1^+$, and also determined the branching fraction ratio

$$\frac{B(E \to K^*\overline{K})}{B(E \to K^*\overline{K} + \delta\pi)} = 0.86 \pm 0.12 \quad .$$

However, it should be pointed out that their E signal is over a relatively large background which has a significant $K^*\overline{K}$ component, so that one should regard this result with caution.

In experiment E110 using the Fermilab multiparticle spectrometer, the reaction

$$\pi^- p \to K_S K^\pm \pi^\mp + X$$

21
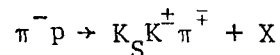
was studied at 50 and 100 GeV/c.[45] Without kinematic cuts, they see

no evidence for an E signal. However, if a δ cut is applied, a

prominent E signal is observed. If a K^* cut is applied rather than

a δ cut, one still sees an E signal, but with considerably more back-

ground. They find a value for the mass of the E of M = 1440 ± 6 MeV.

The width is not well determined because of uncertainties in the

shape of the background. On the surface, this data seems to indicate

a preference for the $\delta\pi$ decay mode of the E over the $K^*\bar{K}$ decay mode.

However, questions of kinematic overlap in the Dalitz plot and phase

space boundaries have not been considered in detail. Thus, this pref-

erence should be considered only as an indication until a more

sophisticated analysis is done.

Despite all the new information on the E from recent experiments,

the situation is not much clearer than it was in 1978. One point of

controversy is whether the E decays predominantly into $\delta\pi$ or $K^*\bar{K}$.

This experiment (and possibly also the Fermilab experiment of Bromberg

et al.[45]) seems to favor the decay E $\rightarrow$ $\delta\pi$. On the other hand,

Dionisi et al.[44] see little evidence for $\delta\pi$ and find the predominant

decay of the E is into $K^*\bar{K}$. As for the spin, Dionisi et al. find

$J^P = 1^+$ which agrees with some earlier results, but disagrees with

others. However, their determination of the spin goes hand-in-hand

with the determination of the predominance of the $K^*\bar{K}$ decay mode.

Since this predominance is not firmly established, I think that one

should still consider the spin of the E to be an open question until

the decay mechanism is understood better.[46]

To understand my reasons for this excessive interest in the

quantum numbers of the E, let me refer for the last time to Fig. 6(b).

As discussed by numerous people,[47] if gluonium states[48] exist, the

process shown in Fig. 6(b), after elimination of the outgoing quark

lines, would be an ideal process for production of such states. I

would like to suggest the possibility that the E might be such a

gluonium state, rather than an ordinary $q\bar{q}$ resonance. Although there

is certainly no real evidence for this hypothesis, there are a few

peculiarities associated with the γE radiative transition from the ψ

which I would like to point out.

First, the branching fraction for $\psi \to \gamma E$ is larger than the corresponding branching fractions for transitions to other ordinary hadrons, with the possible exception of the η'. This is in contrast to hadronic experiments where E production is in general small compared to the production of other resonances. This would lead one to infer a connection between the E and the 2-gluon intermediate state in Fig. 6(b). Whereas the production of gluonium states is expected to be significant in ψ radiative transitions, there is no reason to expect significant production of such states in hadronic reactions.

Second, whereas in most hadronic experiments in which an E is observed to decay into $K\bar{K}\pi$, one observes roughly comparable D(1285) production. Neither this experiment nor the Crystal Ball experiment sees much evidence for D production. We have calculated an upper limit for D production from our data of
$B(\psi \to \gamma D) \times B(D \to K\bar{K}\pi) < 0.7 \times 10^{-3}$ at the 90% confidence level. This might be taken as strong evidence for a difference in the production mechanisms involved in the two different processes, and hence an indication of a large gluonium component in the E. However, if one assumes that the D and E are both members of the standard $J^{PC} = 1^{++}$ nonet, and the E is the primarily singlet state and the D is the primarily octet state,[49] one would expect D production to be suppressed relative to E production because of SU(3) symmetry arguments. Thus, this suppression may not be relevant to the gluonium question at all.

In my opinion, the most important question which should be resolved regarding the E is its spin. If the E can be firmly established as an axial vector state, there is no reason not to make the standard $q\bar{q}$ meson interpretation and put it in the same nonet as the D(1285), A_1, and Q_A. If, on the other hand, the E is finally established as a pseudoscalar, it is difficult to interpret it within the standard quark model. The $J^P = 0^-$ nonet is complete, and one would have to consider the existence of another 0^- nonet, possibly a radial excitation of the ground state, in order to accommodate the E. However, I think it is equally plausible to interpret the E as a gluonium state.

IV. PROPERTIES OF D MESONS

Evidence for production of charmed D mesons by reconstruction of exclusive final states came first from the SLAC–LBL magnetic detector collaboration at SPEAR.[50] I will present some recent results based on a sample of events taken at the ψ''(3772) which corresponds to an integrated luminosity of 2850 nb^{-1}.[51]

In the charmonium model,[52] the ψ'' is presumed to be the $^3D_1$ level of the $c\bar{c}$ system, lying between $D\bar{D}$ and $D\bar{D}^*$ threshold. Because it is less than 100 MeV above the ψ'(3684), but has a total width about two orders of magnitude greater than the ψ' width, the width is generally attributed solely to the strong decay of the resonance into the newly-opened $D\bar{D}$ channel. If the ψ'' has a unique isospin (either 0 or 1), then it couples equally (within phase space factors) to pairs of charged and neutral D mesons. Thus, a measurement of the ψ'' resonant line shape permits a local evaluation of the inclusive D^0 and D^+ production cross sections. Our results from a fine scan over the ψ'' give

$$\sigma_{D^0} = 8.0 \pm 1.0 \pm 1.2 \text{ nb}$$

$$\sigma_{D^+} = 6.0 \pm 0.7 \pm 1.0 \text{ nb}$$

$$(7)$$

at $E_{c.m.} = 3.771$ GeV.[53] The first error is statistical and the second is systematic. Knowledge of these inclusive cross sections allows a determination of absolute branching fractions for observed D decays. In addition, the proximity of the ψ'' to $D\bar{D}$ threshold results in low momentum, 2-body production, which permits a further reduction of background through kinematic constraints.[54]

A.   Exclusive Decays

The branching fractions for various Cabibbo-favored decay modes (i.e., modes containing either one charged or neutral kaon) have been measured.[55] Figure 17 shows the beam energy-constrained invariant mass distributions for the D^0 decays $K^-\pi^+$, $K_S\pi^+\pi^-$, and $K^-\pi^+\pi^+\pi^-$. (For clarity, references to D^0 or D^+ and their decay modes will be assumed to refer to both the state and its charge conjugate.)
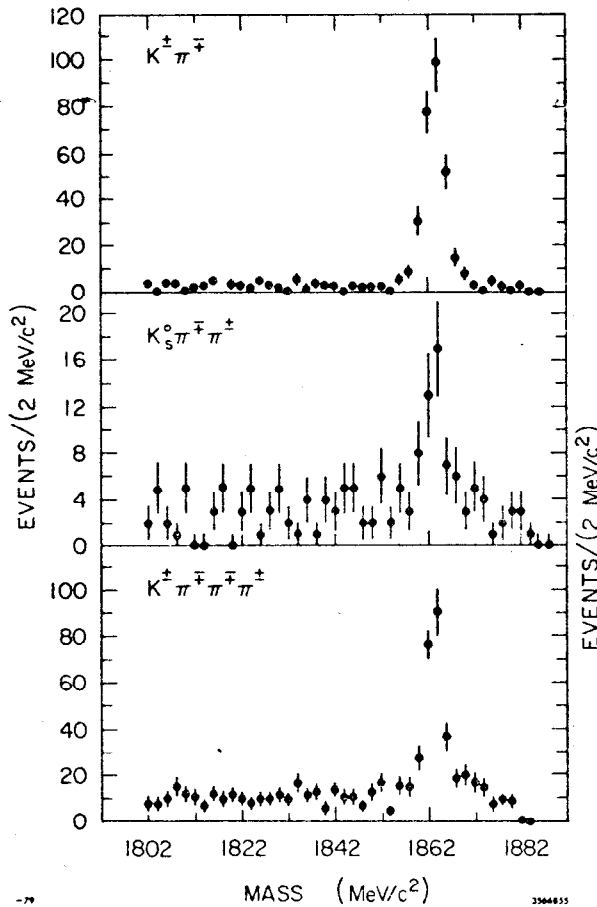
Fig. 17. Beam energy-
constrained invariant
mass distributions for
D^O decays detected in
all charged particle
modes.
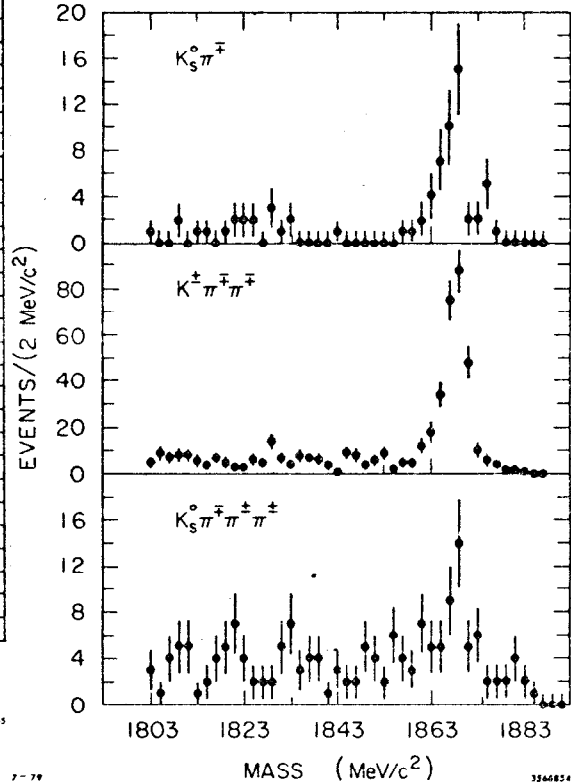
Fig. 18. Beam energy-constrained in-
variant mass distributions for D^+
decays detected in all charged particle
modes.

Figure 18 shows the invariant mass distributions for the D^+ decays $K_S\pi^+$, $K^-\pi^+\pi^+$, and $K_S\pi^+\pi^+\pi^-$. Figure 19 shows the invariant mass distributions for the decays $K_S\pi^O$, $K^-\pi^+\pi^O$, and $K_S\pi^+\pi^O$, each of which contains a single π^O. These distributions provide evidence for the previously unmeasured decays of the D^O into $\overline{K}^O\pi^O$ and D^+ into $\overline{K}^O\pi^+\pi^O$ and $\overline{K}^O\pi^+\pi^+\pi^-$.

Table III gives the calculated branching fractions for these nine decay modes. The detection efficiency for each decay mode was determined by Monte Carlo calculation. Except for the channels $\overline{K}^O\pi^+\pi^-$ and $K^-\pi^+\pi^O$, where the measured resonant substructure in the decay (to be discussed shortly) was used in the Monte Carlo event

25

Fig. 19. Beam energy-constrained invariant mass distributions for D^0 and D^+ detected in modes with a single π^0.
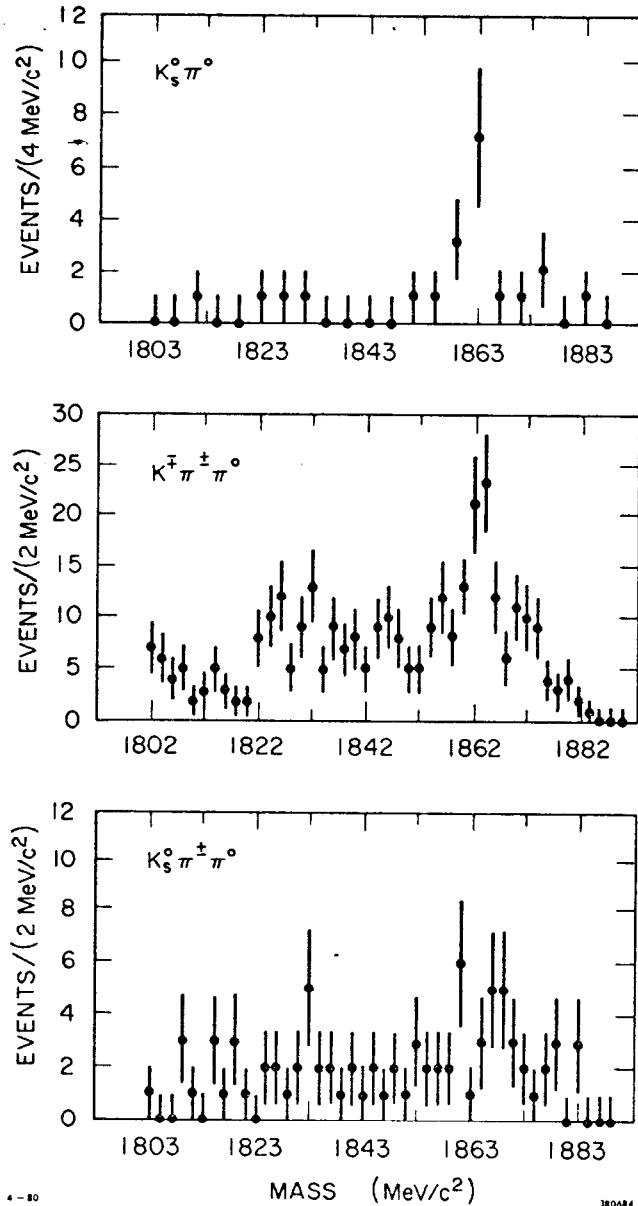
generation, all final states were assumed to follow a uniform phase space distribution. The quoted errors include all systematic sources added in quadrature to the statistical errors which were obtained from fits to the invariant mass distributions. Also shown in Table III are the previously measured branching fractions.[56] It should be noted that the values we find for σ_{D^0} and σ_{D^+}[53] are approximately 30% smaller than those employed in the previous determination of the branching fractions.[56] This should be taken into account when comparing branching fractions from the two experiments.

We have analyzed the Dalitz plot distributions for the $K^-\pi^+\pi^0$ and $\overline{K}^0\pi^+\pi^-$ decays of the D^0 and the $K^-\pi^+\pi^+$ decay of the D^+. The apparently large branching fraction of the D^0 into the $K^-\pi^+\pi^0$ relative to the D^+ decay into $K^-\pi^+\pi^+$ has always been theoretically hard to understand.[57] However, our new results on the resonant substructure in these 3-body decays combined with the apparent difference in total widths of the D^+ and D^0 (to be discussed later) allows a resolution of the problem.[58]

Table III. Branching fractions for Cabibbo-favored D decays.

decay mode	branching fraction (%) Mark II	LGW[a]
$K^-\pi^+$	3.0 ± 0.6	2.2 ± 0.6
$\bar{K}^0\pi^0$	2.2 ± 1.1	--
$\bar{K}^0\pi^+\pi^-$	3.8 ± 1.2	4.0 ± 1.3
$K^-\pi^+\pi^0$	8.5 ± 3.2	12.0 ± 6.0
$K^-\pi^+\pi^+\pi^-$	8.5 ± 2.1	3.2 ± 1.1
$\bar{K}^0\pi^+$	2.3 ± 0.7	1.5 ± 0.6
$K^-\pi^+\pi^+$	6.3 ± 1.5	3.9 ± 1.0
$\bar{K}^0\pi^+\pi^0$	12.9 ± 8.4	--
$\bar{K}^0\pi^+\pi^+\pi^-$	8.4 ± 3.5	--

[a] Ref. 56

Figure 20(a) shows the Dalitz plot for the decay $D^0 \to \bar{K}^0\pi^+\pi^-$. Figure 20(d) shows the low-mass $\bar{K}^0\pi^\pm$ mass-squared projection. One sees a significant population of the K^* bands, but no strong evidence for ρ production. To determine the amount of resonant substructure in the decay, we performed a maximum-likelihood fit to the data in the Dalitz plot. We used a density function which represented the allowed final-state channels plus background, with corrections for detector acceptance made at each point. In the fit, the ρ and K^* amplitudes were represented as p-wave Breit-Wigner line shapes, with energy dependent widths and with the appropriate decay angular distributions. The amplitudes of all indistinguishable resonant final states that were accessible in the decay were allowed to interfere with arbitrary phase. The non-resonant components (i.e., pure 3-body decays and background events) were added incoherently to the density function used in the fit. The fractions of $\bar{K}^0\pi^+\pi^-$ events in each final state (as determined by the fit) are

$$f(K^{*-}\pi^+) = 0.70 \begin{array}{l} +0.13 \\ -0.15 \end{array} \begin{array}{l} +0.05 \\ -0.06 \end{array}$$

$$f(\bar{K}^0\rho^0) = 0.02 \begin{array}{l} +0.08 \\ -0.02 \end{array} \pm 0.03$$

$$f(\bar{K}^0\pi^+\pi^-) = 0.30 \begin{array}{l} +0.16 \\ -0.13 \end{array} \pm 0.05$$

The first set of errors in each case is the statistical error derived from the likelihood function in the fitting procedure. The second set of errors is the estimated systematic uncertainty from the
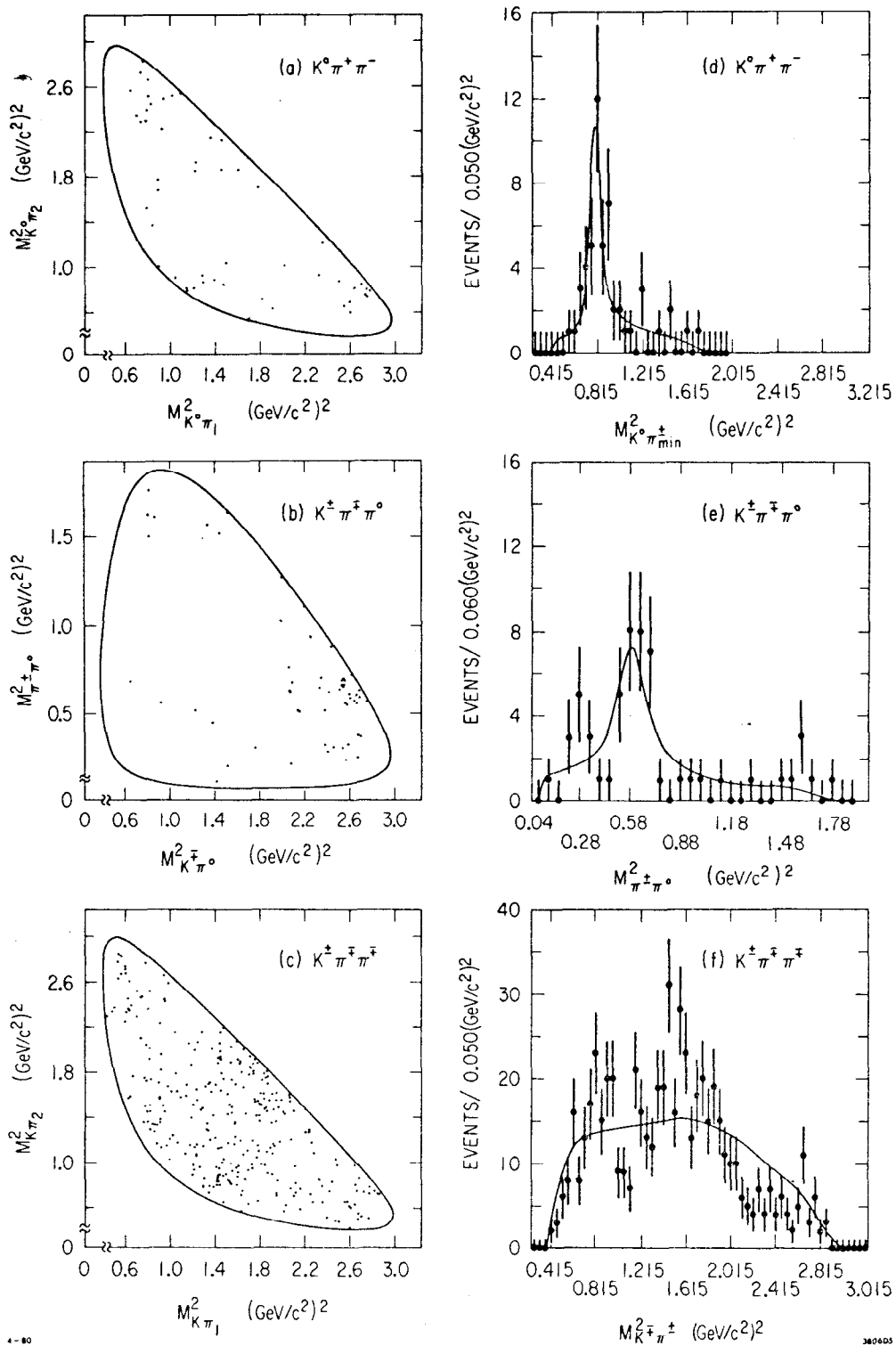
Fig. 20. Dalitz plots for the decays a) $D^0 \to \overline{K}^0 \pi^+ \pi^-$, $D^0 \to K^- \pi^+ \pi^0$, and c) $D^+ \to K^- \pi^+ \pi^+$. Invariant mass-squared projections for d) low-mass $\overline{K}_0 \pi^\pm$ from $\overline{K}^0 \pi^+ \pi^-$, e) $\pi^+ \pi^0$ from $K^- \pi^+ \pi^0$, and f) $K^- \pi^+$ from $K^- \pi^+ \pi^+$. Curves represent fitted solutions discussed in text.

28

Monte Carlo statistics and acceptance calculation, and our assumptions about backgrounds and resonance line shapes. (The values we quote represent the fractions of channels in the absence of interference, and hence the fractions will not necessarily sum to unity.) The curve in Fig. 20(d) represents the fitted solution.

Figure 20(b) shows the $K^-\pi^+\pi^0$ Dalitz plot, with $\pi^+\pi^0$ mass-squared projection shown in Fig. 20(e). The ρ peak is evident in the $\pi^+\pi^0$ mass projection, but it is only seen on the right side of the Dalitz plot. One would expect the ρ band to extend across the plot from one boundary to the opposite boundary. However, the π^0 detection efficiency varies rapidly from the upper right edge of the plot (where it is relatively large) to the lower left corner (where it is very small). This results in good detection efficiency for ρ's only near the right side of the Dalitz plot. The results of a fit to the Dalitz plot (done in an identical manner to that for the previous Dalitz plot) are

$$f(K^-\rho^+) = 0.85 \begin{array}{c} +\ 0.05 \\ -\ 0.11 \end{array} \begin{array}{c} +\ 0.09 \\ -\ 0.10 \end{array}$$

$$f(\bar{K}^{*0}\pi^0) = 0.11 \begin{array}{c} +\ 0.12 \\ -\ 0.06 \end{array} \pm\ 0.10$$

$$f(K^{*-}\pi^+) = 0.07 \begin{array}{c} +\ 0.06 \\ -\ 0.04 \end{array} \begin{array}{c} +\ 0.05 \\ -\ 0.02 \end{array}$$

$$f(K^-\pi^+\pi^0) = 0.06 \pm 0.04 \pm 0.05$$

An independent estimate for the $K^{*-}\pi^+$ fraction of this decay mode can be made from the measured $K^{*-}\pi^+$ fraction of the $\bar{K}^0\pi^+\pi^-$ decay, the $K^-\pi^+\pi^0$ and $\bar{K}^0\pi^+\pi^-$ branching fractions from Table III, and the charged K^* branching fractions. We expect a value of $f(K^{*-}\pi^+) = 0.15 \pm 0.07$, which is consistent with the fraction obtained from the direct fit to the $K^-\pi^+\pi^0$ Dalitz plot.

The Dalitz plot for the $K^-\pi^+\pi^+$ decay of the D^+ is shown in Fig. 20(c). Our large sample (292 events with an estimated background of approximately 12%) provides the first evidence for a non-uniform population of the Dalitz plot. The detection efficiency is very uniform across the plot, dropping only near the three corners where π

and K momenta fall below approximately 100 MeV/c. Figure 20(f) shows the sum of the two $K^-\pi^+$ invariant mass-squared combinations and a curve indicating the distribution expected for a purely uniform phase space decay. While no evidence for a significant K^* signal exists, we note again the large deviation of the data from uniform phase space. We present only an upper limit on the $\bar{K}^{*0}\pi^+$ channel in this decay by assuming that all of the events observed in the resonance region ($0.685 \leq M_{K\pi} < 0.905$ GeV^2) arise from the decay $\bar{K}^{*0}\pi^+$. This assumption results in a 90% c.l. upper limit of 0.39 for the fraction of this decay mode in $\bar{K}^{*0}\pi^+$. (Additional systematic errors may change this limit by ±0.06.)

B. Inclusive Properties

The uniqueness of the $D\bar{D}$ final state at the ψ'' provides a means of studying the inclusive properties of D decays by use of "tagged" events. In a tagged event, one D ($\bar{D}$) is identified by the observed decay into $\bar{K}^0\pi^+$, $K^-\pi^+$, $K^-\pi^+\pi^+$, or $K^-\pi^+\pi^-\pi^+$. The recoiling system provides a pure $\bar{D}$ (D) sample. This sample of D's is unbiased by the trigger requirement which is satisfied in all cases by the tagged D. Cuts on the beam energy-constrained masses of ±6 MeV around the nominal D mass (±4 MeV in the case of the $K^-\pi^+\pi^-\pi^+$ decay mode) were made to select the sample of tagged events used in the analysis. The resulting sample consists of approximately 300 D^+ and 480 D^0 events over a background equal to about 12% of the signal. In this section, I will discuss the inclusive charged particle multiplicity and strangeness associated with D decays. In the next section, I will discuss the individual D^0 and D^+ semileptonic decay fractions.

For each tag, the multiplicity observed in the recoiling system is plotted, with no attempt at particle identification. (For this analysis only, no $\bar{K}^0\pi^+$ tags were used.) These observed charged particle multiplicity distributions are shown in Figs. 21(a)-(c). The shaded regions represent the background multiplicity distributions estimated from events with invariant mass between 1.800 and 1.855 GeV, normalized to the expected number of background events contaminating the tagged D sample. The produced charged particle multiplicity distributions (where $K^0 \rightarrow \pi^+\pi^-$ decays are counted as two tracks)
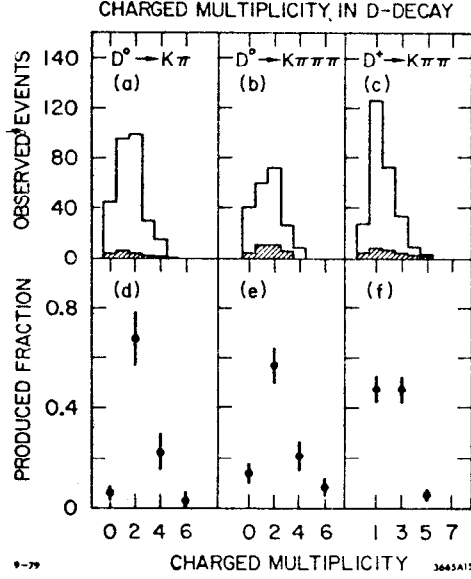
CHARGED MULTIPLICITY IN D-DECAY

Fig. 21. Observed charged particle multiplicity distributions for a) $D^0 \to K^- \pi^+$, b) $D^0 \to K^- \pi^+ \pi^+ \pi^-$, and c) $D^+ \to K^- \pi^+ \pi^+$ tagged events. Produced (unfolded) charged particle multiplicity distributions for d) $D^0 \to K^- \pi^+$, e) $D^0 \to K^- \pi^+ \pi^+ \pi^-$, and f) $D^+ \to K^- \pi^+ \pi^+$ tagged events. Shaded regions are discussed in text.

were obtained by a numerical unfold procedure.[59] Briefly, a solution is sought for $\tilde{N}_p$ in the over-constrained linear system of equations

$$N_q = \sum_p \varepsilon_{qp} \tilde{N}_p + B_q \quad ,$$

where N_q is the number of events detected with q charged prongs, $\tilde{N}_p$ is the number of events produced with p charged prongs, B_q is the number of background events with q charged prongs, and ε_{qp} is the probability (determined by Monte Carlo) that a produced event with p prongs will be detected with q prongs. The produced (unfolded) multiplicity distributions are shown in Figs. 21(d)-(f), where the error bars reflect only the statistics of the unfold procedure. The systematic errors are comparable. The mean charged particle multiplicities are calculated to be $\langle N_{ch} \rangle_{D^0} = 2.46 \pm 0.14$ (based on both samples of D^0 tags) and $\langle N_{ch} \rangle_{D^+} = 2.16 \pm 0.16$, where the errors include estimates of the systematic uncertainties. These results are in good agreement with the previously reported value for $\langle N_{ch} \rangle$ of 2.3 $\pm$ 0.3 for both the D^0 and D^+.[60]

Theoretical estimates of the average D multiplicities have generally been larger than these measured values.[61] However, at least one type of statistical model discussed by Quigg and Rosner[61] (the constant-matrix-element model) predicts average multiplicities which are close to the experimental values. They predict $\langle N_{ch} \rangle_{D^0} = 2.4$ and $\langle N_{ch} \rangle_{D^+} = 2.5$ for hadronic decays of the D.

31

However, it should be noted that our measurements include contributions from the semileptonic decays, which comprise a large fraction of the D^+ decays (as will be discussed in the next section). If a large fraction of the semileptonic decays are $D^+ \rightarrow K^0 \ell^+ \nu_\ell$, one would expect a smaller average multiplicity for D^+ decays than for D^0 decays, as is observed in the data.

The tagged D samples were chosen to have unique strangeness, so that charged kaons in the recoiling system could be characterized as having either the same or opposite strangeness. The Cabibbo-favored decays should produce one kaon whose strangeness is opposite that of the tag, while Cabibbo-suppressed decays are expected to exhibit either no strange particles, or two of opposite strangeness. $D^0 - \overline{D}^0$ mixing and doubly suppressed decays can produce a particle with strangeness equal to the strangeness of the kaon in the tag, but these effects are expected to be very small.[62]

Table IV summarizes the results of an analysis to determine the kaon fractions in the systems recoiling against the tagged D's. These numbers have been corrected for kaon detection efficiency, misidentification of $\pi^\pm$ as $K^\pm$, and kaons from the background events which

Table IV. Kaon multiplicities in D decays.

| decay mode | branching fraction (%) | | experiment |
	D^0	D^+	
$D \rightarrow K^- X$	56 ± 11	19 ± 5	Mark II
	36 ± 10[a]	10 ± 7	LGW[b]
$D \rightarrow K^+ X$[c]	8 ± 3	6 ± 4	Mark II
	--[a]	6 ± 6	LGW[b]
$D \rightarrow K^0 X$[d]	29 ± 11	52 ± 18	Mark II
	57 ± 26	39 ± 29	LGW[b]

[a] The LGW did not separate the same-strangeness and opposite-strangeness events; both are combined under $D \rightarrow K^- X$.

[b] Ref. 60.

[c] These decays have kaons with the same strangeness as the kaon in the tag.

[d] Here the strangeness cannot be determined.

contaminate the tagged D sample. The errors include both statistical errors and estimated systematic errors. Also shown in Table IV is a comparison of our results with those of Ref. 60.

It is expected that if one could extract from the data the sample of events that correspond only to Cabibbo-favored decays, the kaon fraction (including both charged and neutral kaons) should be 100%. This is not possible, but one can make assumptions about the Cabibbo-suppressed decays, and estimate this fraction. If it is assumed that $B(D \to \overline{K}K + n\pi) \approx 0.05$[63] and $B(D \to \pi\text{'s only}) \approx 0.05$, one finds that $86 \pm 17\%$ of Cabibbo-favored D^o decays contain a kaon and $70 \pm 21\%$ of Cabibbo-favored D^+ decays contain a kaon. These numbers were derived independently of the measured wrong-sign kaon fractions, and the errors do not include systematic uncertainties in the assumptions made about the fraction of Cabibbo-suppressed decays.

C. Semileptonic D Decays and the D Lifetime

The pure leptonic decays of D mesons are expected to be strongly suppressed relative to the semileptonic decays,[62] implying that electrons originating from D decays will come predominantly from the semileptonic modes. Previous experiments[64] have measured the average semileptonic branching ratios for D mesons[65] at several center-of-mass energies in e^+e^- annihilations. However, until recently, no measurements of the individual semileptonic branching fractions of the D^o and D^+ have been made. Whereas it is expected that the semileptonic partial widths of the D^o and D^+ are approximately equal,[66] there is no overriding reason to expect that the total D^o and D^+ widths are equal. This inequality in the total widths would lead to a difference in the D^o and D^+ semileptonic branching fractions. Hence, a measurement of the ratio of the two semileptonic branching fractions allows an estimate of the relative lifetimes to be made

$$\frac{\tau_{D^+}}{\tau_{D^o}} = \frac{B(D^+ \to Xe\nu)}{B(D^o \to Xe\nu)} \quad .$$

In order to measure the D^o and D^+ semileptonic branching fractions, the sample of tagged events described in the previous section was searched for electron candidates. All events with electron candidates were hand scanned to remove visible photon

33

conversions. All remaining tracks were separated by charge relative to the strangeness of the tag. We denote these two groups as "right-sign" (having the expected leptonic charge) and "wrong-sign" (having opposite the expected leptonic charge) candidates. Possible backgrounds were carefully considered. Backgrounds arising from hadronic misidentification are charge asymmetric (i.e., the right-sign and wrong-sign backgrounds differ) and strongly correlated with the strangeness of the tagged D. To estimate this background, the measured D-decay momentum distributions were folded with the known hadron misidentification probabilities to estimate the contamination in each group of electrons. Backgrounds from electromagnetic processes are charge symmetric and uncorrelated with the strangeness of the tagged D. This background was corrected for, after corrections for all other backgrounds were made, by subtracting the wrong-sign rate from the right-sign rate to get the net electron rate. Contamination from leptonic kaon decays was estimated to be negligible. Contamination of the tagged D sample was estimated from events below the D mass ($1.800 \leq M_{tag} < 1.855$ GeV) and corrections made for this. Finally, some $K^-\pi^+$ events were mislabeled as π^-K^+, which gave an incorrect strangeness assignment. Monte Carlo estimates were used to correct for this contamination.

A summary of the semileptonic rate calculation is shown in Table V. After correction of the number of net semileptonic events for detection efficiency and the number of tags, we find

$$B(D^+ \to Xe\nu) = 16.8 \pm 6.4\%$$

$$B(D^o \to Xe\nu) = 5.5 \pm 3.7\% \quad .$$

While these values are dominated by the statistical errors, they also include our estimates of the systematic errors. Weighting these values by the relative D^o and D^+ production cross sections at the ψ'' (7), we obtain an average single electron branching fraction of $10.0 \pm 3.2\%$. This is consistent with $8.0 \pm 1.5\%$ measured by DELCO[64] and $7.2 \pm 1.8\%$ measured by the LGW[64] at the same center-of-mass energy.

Table V. D semileptonic rate calculation.

$D^o - K^-\pi^+$ and $K^-\pi^+\pi^-\pi^+$ tags	
net tagged events	477
right-sign electrons observed[a]	36
background[b]	17.4 ± 1.0
wrong-sign electrons observed[a]	18
background[b]	11.8 ± 0.9
additional backgrounds[c]	-0.1 ± 1.0
net electrons	12.3 ± 7.6

$D^+ - \bar{K}^o\pi^+$ and $K^-\pi^+\pi^+$ tags	
net tagged events	295
right-sign electrons observed[a]	39
background[b]	16.3 ± 1.0
wrong-sign electrons observed[a]	4
background[b]	4.2 ± 0.5
additional backgrounds[c]	0.5 ± 0.8
net electrons	23.3 ± 6.7

[a] Particles satisfying electron cuts.

[b] Expected background from hadron misidentification.

[c] Net background from mislabeled $K^-\pi^+$ tags and false tags.

In the ratio, there is a cancellation of some of the systematic errors and we obtain

$$\frac{\tau_{D^+}}{\tau_{D^o}} = 3.1^{+4.6}_{-1.4} \quad . \quad (8)$$

This ratio was obtained by performing a maximum-likelihood fit to the relative rates. Figure 22 shows the logarithm of the likelihood as a function of the ratio τ_{D^+}/τ_{D^o}. The errors in (8) represent $\pm 1\sigma$ about 3.1, assuming a local Gaussian form for the likelihood function. Statistically, a change of approximately 2σ is required to obtain equal lifetimes, while the upper limit is poorly defined because of the small number of observed semileptonic D^o decays.

The DELCO collaboration has recently made a measurement of the individual semileptonic branching fractions of the D^+ and D^o based on a measurement of the number of ψ'' decays containing either one or two electrons originating from semileptonic decays of D mesons.[67] The values of the D^o and D^+ semileptonic branching fractions (b^o and b^+, respectively) were determined by finding a common solution to the pair of equations

$$N_{1e} = N_o \, \varepsilon_1^o \, 2b^o(1 - b^o) + N_+ \, \varepsilon_1^+ \, 2b^+(1 - b^+) + \text{smaller terms in } b^2$$

$$N_{2e} = N_o \, \varepsilon_2^o(b^o)^2 + N_+ \, \varepsilon_2^+(b^+)^2 \quad,$$

where N_{1e} and N_{2e} are the number of observed one-electron and two-electron events and N_o and N_+ are the number of $D^o\overline{D}^o$ and D^+D^- decays in the data sample. The efficiency ε_1^o (ε_1^+) is the probability of detecting a 1e event from a $D^o\overline{D}^o$ (D^+D^-) initial state in which one D decays to an electron. ($\varepsilon_2^{o,+}$ are defined similarly for 2e events.) They determine

$$B(D^+ \to Xe\nu) = 22.0 \begin{array}{c} + 4.4 \\ - 2.2 \end{array} \%$$

$$B(D^o \to Xe\nu) < 4.0\% \text{ (95\% c.l.)} \quad.$$

These values imply that the ratio of lifetimes is

$$\frac{\tau_{D^+}}{\tau_{D^o}} > 4.3 \text{ (95\% c.l.)} \quad.$$

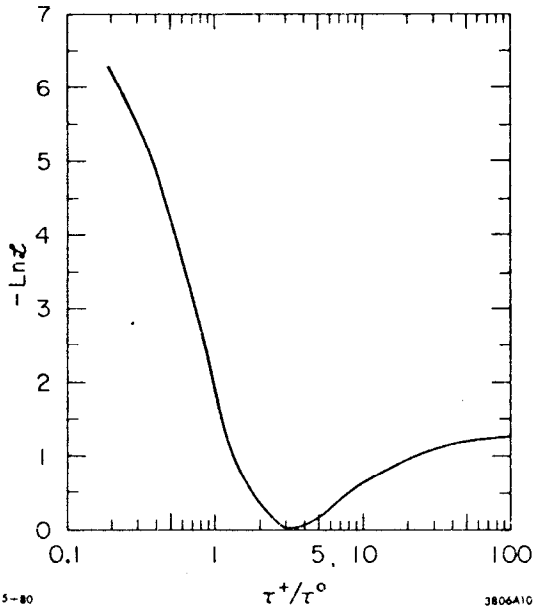These branching fractions are consistent with the values determined by the Mark II.

Fig. 22. Logarithm of the likelihood function versus the ratio of the D^+ and D^o total lifetimes.

Based on our branching fraction measurements, the theoretical estimate for the partial width $\Gamma(D \to Ke\nu) = 1.4 \times 10^{11} \text{ sec}^{-1}$,[68] and the assumption[69]

$$\frac{\Gamma(D \to Ke\nu)}{\Gamma(D \to Xe\nu)} = 0.6 \quad,$$

we estimate the D^+ and D^o lifetimes

$$\tau_{D^+} \approx 7.2 \times 10^{-13} \text{ sec}$$

$$\tau_{D^o} \approx 2.4 \times 10^{-13} \text{ sec} \quad.$$

These estimates compare well with measured lifetimes from the

Fermilab neutrino experiment E531 in which 5 D^+ and 7 D^o candidates have been observed to decay in emulsion.[70] They measure the lifetimes to be $\tau_{D^+} = 10.3 \begin{smallmatrix} + 10.5 \\ - 4.1 \end{smallmatrix} \times 10^{-13}$ sec and $\tau_{D^o} = 1.00 \begin{smallmatrix} + 0.52 \\ - 0.31 \end{smallmatrix} \times 10^{-13}$ sec.

V. $\tau \to K^*(890)\nu_\tau$

The properties of the heavy lepton τ^- have been carefully studied in a number of experiments.[71] I would like to briefly discuss the decay $\tau^- \to K^{*-}(890)\nu_\tau$ (for simplicity, all references to τ^- imply also the charge conjugate state) which has been observed by the Mark II collaboration. This is the first observation of a Cabibbo-suppressed τ decay.

Figure 23 compares the W-exchange diagrams for the processes $\tau \to K^*\nu_\tau$ and $\tau \to \rho\nu_\tau$. The diagrams are identical except for the coupling of the W to the final-state hadron in each case, where the K^* final state is Cabibbo-suppressed (i.e., the coupling is proportional to $\sin^2\theta_c$) and the ρ final state is Cabibbo-favored (with coupling proportional to $\cos^2\theta_c$). There is no reason not to expect θ_c to be the standard Cabibbo angle.[72]

Our analysis was based on a sample of 40,200 $\tau^+\tau^-$ pairs produced with $E_{c.m.} > 4.2$ GeV. The decay sequence which was analyzed was
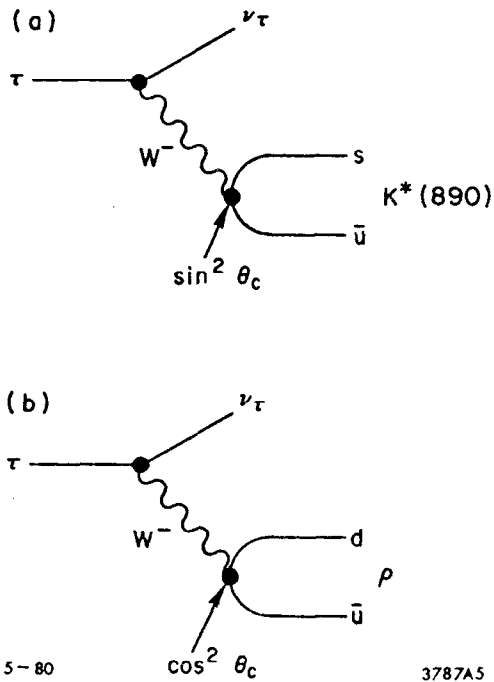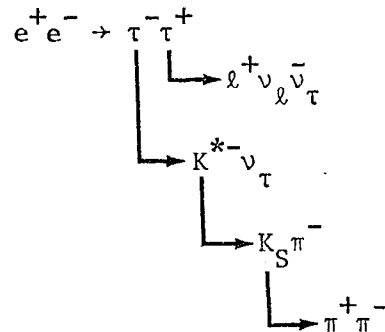

We required four charged particles in the final state, one of which was identified as an e or a μ.

Fig. 23. Diagrams for
a) $\tau \to K^*(890)\nu_\tau$ and b) $\tau \to \rho\nu_\tau$.

Events in which any of the other three tracks were identified as leptons, kaons, or protons were eliminated. Events with an observed photon with energy greater than 100 MeV were also eliminated.[73] Finally, it was required that two of the oppositely charged pions reconstruct in space to form a secondary vertex at a distance of at least 1 cm from the primary decay point and have a mass consistent with the nominal K^o mass ($0.465 \leq M_{\pi^+\pi^-} < 0.510$ GeV).

Figure 24 shows the invariant mass spectrum for the $K_S\pi^\pm$ events selected above. There are 11 signal events (with $0.825 \leq M_{K\pi} < 0.950$ GeV) with an estimated background of 2.5 events (determined from events in the regions $0.700 \leq M_{K\pi} < 0.825$ GeV and $0.950 \leq M_{K\pi} <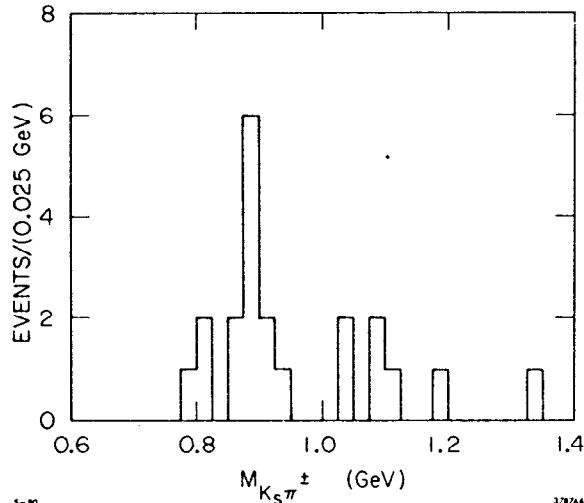 1.075$ GeV). The detection efficiency was calculated by Monte Carlo separately for the events with an e and the events with a μ, yielding $\varepsilon_{eK}* = 2.1\%$ and $\varepsilon_{\mu K}* = 1.4\%$. Seven of the eleven events observed in the signal region were electron events. As the statistics were too limited to estimate what fraction of the subtracted background events were electron events, the 8.5 ± 3.6 corrected events were scaled by 7/11 to give the number of corrected electron events and 4/11 to give the number of corrected muon events.

Fig. 24. $K_S\pi^\pm$ invariant mass distribution in candidate events for $\tau \to K^*(890)\nu_\tau$.

The branching fractions were calculated separately for the e and μ event samples according to the prescription

$$N_\ell = 2\varepsilon_{\ell K}* \ B(\tau \to K^*\nu_\tau) \times B(\tau \to \ell\bar{\nu}_\ell\nu_\tau) \ .$$

For the leptonic branching fraction, we used a value $B(\tau \to \ell\bar{\nu}\nu_\tau) = 18.5 \pm 1.5\%$ obtained from analysis of eμ events in

the same data sample. Our best estimate for $B(\tau \to K^* \nu_\tau)$ is a weighted average of the two determinations:

$$B(\tau \to K^* \nu_\tau) = 1.6 \pm 0.8\% \quad .$$

This branching fraction can be compared with theoretical estimates based on the measured branching fraction for $\tau \to \rho \nu_\tau$ of $20.5 \pm 4.1\%$ from our experiment.[74] Based on calculations of Tsai[72]

$$\frac{B(\tau \to K^*(890)\nu_\tau)}{B(\tau \to \rho\nu_\tau)} = f(M_\tau, M_\rho, M_{K^*}) \cdot \tan^2\theta_c \quad ,$$

where f is a phase space factor and is approximately 0.93. The value used for the Cabibbo angle is $\sin^2\theta_c = 0.07$ rather than the customary value of $\sin^2\theta_c = 0.05$ in order to take into account the difference between the coupling constants f_K and f_π.[75] From this, we expect $B(\tau \to K^*\nu_\tau) = 1.4 \pm 0.4\%$ which is in good agreement with the experimental measurement.

VI. CONCLUSIONS

I have presented some recent results from three different areas of e^+e^- annihilation physics. The first part of the talk dealt with radiative transitions from the ψ to ordinary hadrons. The new results on the η, η', and f confirm earlier results, but there is still a possible factor-of-two discrepancy involved with the $\psi \to \gamma\eta'$ branching fraction. I tried to emphasize that these transitions can be understood in terms of minimal gluon-coupling ideas, with mixing between the different isoscalar states in the SU(4) multiplet playing a fundamental role in quantitatively understanding the results. The results on the $\gamma E(1420)$ transition are particularly interesting as the possibility exists that the E is a gluonium state. However, it is doubtful whether it will ever be possible to show convincing evidence for this interpretation.

Although it was not emphasized during the talk, there has been some effort by the Mark II collaboration to look for other radiative transitions from the ψ. All states with reasonable acceptance in the Mark II detector (i.e., states decaying into combinations of $\pi^\pm$, $K^\pm$, K_S, p, and $\bar{p}$), and even some with poor acceptance (e.g., states with

π^o's or η's in the final state), have been considered. No statistically significant signals aside from those shown today have been observed. Thus, if the E is not a gluonium state, neither the Mark II nor the Crystal Ball sees any evidence for such a state in radiative transitions from the ψ.[76]

A significant amount of information on the properties of D mesons has come from the Mark II, only part of which could be discussed here. In terms of exclusive channels, a few new decay modes have been observed, and a detailed analysis of the resonant substructure of the $K\pi\pi$ decay modes has been made. These results are important in understanding the mechanisms involved in D decays. Of the inclusive properties discussed, the most interesting is the result on the D^o and D^+ semileptonic decays rates. The combined results from the Mark II, DELCO, and the ν emulsion experiments provide fairly conclusive evidence that the D^+ lifetime is considerably longer than the D^o lifetime.

Finally, the measured branching fraction for $\tau \to K^* \nu_\tau$ is consistent with expectations from standard Cabibbo theory.

REFERENCES

1. Members of the SLAC-LBL Mark II collaboration: G. Abrams, M. Alam, C. Blocker, A. Boyarski, M. Breidenbach, D. Burke, W. Carithers, W. Chinowsky, M. Coles, S. Cooper, W. Dieterle, J. Dillon, J. Dorenbosch, J. Dorfan, M. Eaton, G. Feldman, M. Franklin, G. Gidal, G. Goldhaber, G. Hanson, K. Hayes, T. Himel, D. Hitlin, R. Hollebeek, W. Innes, J. Jaros, P. Jenni, D. Johnson, J. Kadyk, A. Lankford, R. Larsen, V. Lüth, R. Millikan, M. Nelson, C. Pang, J. Patrick, M. Perl, B. Richter, A. Roussarie, D. Scharre, R. Schindler, R. Schwitters, J. Siegrist, J. Strait, H. Taureg, M. Tonutti, G. Trilling, E. Vella, R. Vidal, I. Videau, J. Weiss, and H. Zaccone.
    Members of the Crystal Ball collaboration. California Institute of Technology, Physics Department: R. Partridge, C. Peck and F. Porter. Harvard University, Physics Department: D. Andreasyan, W. Kollman, M. Richardson, K. Strauch and K. Wacker. Princeton University, Physics Department: D. Aschman, T. Burnett,

M. Cavalli-Sforza, D. Coyne, M. Joy and H. Sadrozinski. Stanford Linear Accelerator Center: E. D. Bloom, F. Bulos, R. Chestnut, J. Gaiser, G. Godfrey, C. Kiesling, W. Lockman and M. Oreglia. Stanford University, Physics Department and High Energy Physics Laboratory: R. Hofstadter, R. Horisberger, I. Kirkbride, H. Kolanoski, K. Koenigsmann, A. Liberman, J. O'Reilly and J. Tompkins.

2. D. Coyne, invited talk this conference.

3. J.-E. Augustin et al., Phys. Rev. Lett. 34, 233 (1975; J.-E. Augustin et al., Phys. Rev. Lett. 34, 764 (1975).

4. W. Davies-White et al., Nucl. Instrum. Methods 160, 227 (1979).

5. This measurement error is obtained when the tracks are constrained to pass through the known beam position.

6. G. S. Abrams et al., IEEE Trans. Nucl. Sci. 25, 309 (1978).

7. Neutral pions are reconstructed from pairs of γ's detected in the LA. Pairs with invariant mass between 0.075 and 0.200 GeV are considered to be π^o candidates. The π^o signal is extracted after subtraction of the combinatorial background.

8. R. L. Ford and W. R. Nelson, Stanford Linear Acclerator Center Report No. SLAC-210 (1978), unpublished.

9. H. Brafman et al., Stanford Linear Accelerator Center Report No. SLAC-PUB-2033 (1977), unpublished.

10. This process is not related to any physics I will discuss in this talk. I show this particular event only because of the striking similarity between this event and an event observed in the Mark I detector approximately five years earlier [see Fig. 3 in G. S. Abrams et al., Phys. Rev. Lett. 34, 1181 (1975)].

11. G. S. Abrams et al., Phys. Rev. Lett. 44, 114 (1980); D. L. Scharre et al., Stanford Linear Accelerator Center Report No. SLAC-PUB-2513 (1980), to be submitted for publication.

12. M. T. Ronan et al., Phys. Rev. Lett. 44, 367 (1980).

13. Details of the experimental apparatus can be found in E. D. Bloom, in Proceedings of the Fourteenth Rencontre de Moriond, Vol. II, edited by Trân Thanh Vân (R.M.I.E.M. Orsay, 1979), p. 175; and C. W. Peck et al., California Institute of Technology Report

No. CALT-68-753 to be published in the Proceedings of the Annual
Meeting of the American Physical Society, Division of Particles
and Fields, McGill University, Montreal, Canada, October 25-27,
1979.

14. D. G. Aschman, to be published in the Proceedings of the
Fifteenth Rencontre de Moriond, Les Arcs, France, March 15-21,
1980.

15. W. Bartel et al., Phys. Lett. 66B, 489 (1977).

16. W. Braunschweig et al., Phys. Lett. 67B, 243 (1977).

17. R. Partridge et al., Phys. Rev. Lett. 44, 712 (1980).

18. W. Bartel et al., Phys. Lett. 64B, 483 (1976).

19. D. L. Scharre et al., Stanford Linear Accelerator Center Report
No. SLAC-PUB-2514 (1980), to be submitted for publication.

20. G. Alexander et al., Phys. Lett. 72B, 493 (1978).

21. R. Brandelik et al., Phys. Lett. 74B, 292 (1978).

22. W. Braunschweig et al., Phys. Lett. 63B, 487 (1976).

23. B. Jean-Marie et al., Phys. Rev. Lett. 36, 291 (1976).

24. H. Fritzsch and J. D. Jackson, Phys. Lett. 66B, 365 (1977).

25. Because of the six-fold symmetry of the final state, the Dalitz
plot has been folded. This results in the observed folding of
the η and η' bands at the boundary.

26. D. L. Scharre, in Proceedings of the Fourteenth Rencontre de
Moriond, Vol. II, edited by Trân Thanh Vân (R.M.I.E.M. Orsay,
1979), p. 219.

27. However, due to problems with the LA shower counter system,
there was no photon detection for approximately half of the ψ
running time. Thus, any analyses which required photon detection
were based on half of the total data sample.

28. Due to noise in the LA electronics, spurious photons were occa-
sionally reconstructed by the tracking program. In order not to
lose good events, extra photons were allowed in candidate events.
When analyzing these events, separate fits were attempted for
each two-photon combination.

29. In general, two or more charged tracks were required to trigger
the detector.

30. Approximately one million ψ' events were taken. From this sample, 92,000 ψ decays were identified by missing mass from the $\pi^+\pi^-$ system.

31. This ratio is expected to be roughly the same as the ratio of the leptonic branching fractions of the ψ' and ψ.

32. J. Burmester et al., Phys. Lett. 72B, 135 (1977), F. Vanucci et al., Phys. Rev. D 15, 1814 (1977).

33. C. Zaiser et al., in preparation.

34. It is expected that the mixing due to gluon exchange will not affect this ratio as severely as in the case of the pseudoscalar nonet.

35. Particle Data Group, Phys. Lett. 75B, 1 (1978) and references therein.

36. P. Baillon et al., Nuovo Cimento 50A, 393 (1967).

37. This distribution includes a few additional events corresponding to the process $\psi' \to \pi^+\pi^-\psi$, $\psi \to \gamma E$. Details can be found in Ref. 19.

38. The mass resolution of these constrained events is considerably smaller than the natural line width of the resonance and is ignored in the fit.

39. The efficiency used in the determination of this branching fraction was based on a Monte Carlo analysis which assumed all decay distributions were isotropic. If the spin-parity of the E were 0^-, which results in a $1 + \cos^2\theta$ distribution for the angle of the photon with respect to the beam axis, the branching ratio product should be increased by 19%.

40. The increase in sample size arises principally from the fact that the sample of data in which the LA system was not operational could be used.

41. Monte Carlo analysis shows the acceptance to be roughly flat over the entire Dalitz plot. Hence, the observed structure is not the result of variations in the acceptance.

42. This decay mode is expected to be half the $K_S K^{\pm}\pi^{\mp}$ mode by isospin conservation.

43. The correction was based on the $K_S K^\pm$ mass distribution for the sample of $E \to K_S K^\pm \pi^\mp$ events from the Mark II.

44. C. Dionisi et al., CERN Report No. CERN/EP 80-1 (1980), submitted to Nucl. Phys. B.

45. C. Bromberg et al., California Institute of Technology Report No. CALT-68-747 (1980).

46. It has been suggested that the resonance seen in hadronic experiments and known as the E(1420) is not the same state that has been observed by us in radiative transitions from the ψ. However, because of the consistency of the parameters of the states seen in these two processes and the outward similarity of the Dalitz plots, I think it is logical to consider them to be the same state until some evidence to the contrary is produced.

47. See for example J. Donoghue, to be published in the Proceedings of the VI International Conference on Experimental Meson Spectroscopy, Brookhaven National Laboratory, Upton, New York, April 25-26, 1980.

48. A gluonium state is a bound state of two or more gluons.

49. Unfortunately, the masses of the other members of the nonet (the A_1 and the Q_A) are not well enough known to provide a reliable estimate of the mixing angle.

50. G. Goldhaber et al., Phys. Rev. Lett. <u>37</u>, 255 (1976); I. Peruzzi et al., Phys. Rev. Lett. <u>37</u>, 569 (1976).

51. R. H. Schindler et al., Stanford Linear Accelerator Center Report No. SLAC-PUB-2507 (1980), to be submitted for publication.

52. See for example, E. Eichten et al., Phys. Rev. Lett. <u>34</u>, 369 (1975); E. Eichten et al., Phys. Rev. D <u>21</u>, 203 (1980).

53. R. H. Schindler et al., Phys. Rev. D <u>21</u>, 2716 (1980).

54. The energy of the D can be constrained to the beam energy, which results in a significant improvement in the mass resolution.

55. We have previously reported measurements of the Cabibbo-suppressed decay modes $K^- K^+$ and $\pi^+ \pi^-$ in G. S. Abrams et al., Phys. Rev. Lett. <u>43</u>, 477 (1979).

56. I. Peruzzi et al., Phys. Rev. Lett. <u>39</u>, 1301 (1977); D. L. Scharre et al., Phys. Rev. Lett. <u>40</u>, 74 (1978).

57. See for example, M. Matsuda et al., Prog. Theor. Phys. $\underline{59}$, 1396 (1978).

58. The theoretical interpretation of our results is discussed in detail by M. Chanowitz, invited talk this conference.

59. R. H. Schindler, Stanford Linear Accelerator Center Report No. SLAC-219, Ph.D. Thesis, Stanford University, 1979 (unpublished).

60. V. Vuillemin et al., Phys. Rev. Lett. $\underline{41}$, 1149 (1978).

61. See for example, C. Quigg and J. L. Rosner, Phys. Rev. D $\underline{17}$, 239 (1978); M. Peshkin and J. L. Rosner, Nucl. Phys. $\underline{B122}$, 144 (1977).

62. M. K. Gaillard, B. W. Lee, and J. L. Rosner, Rev. Mod. Phys. $\underline{47}$, 277 (1975).

63. It is assumed that decays with K^+K^- and $K^0\bar{K}^0$ are produced equally.

64. R. Brandelik et al., Phys. Lett. $\underline{70B}$, 387 (1977); J. M. Feller et al., Phys. Rev. Lett. $\underline{40}$, 274 (1978); W. Bacino et al., Phys. Rev. Lett. $\underline{43}$, 1073 (1979); J. M. Feller et al., Phys. Rev. Lett. $\underline{40}$, 1677 (1978).

65. At center-of-mass energies above F^+ or Λ_c^+ threshold, there will be some contamination from the semileptonic decays of these other charmed particles.

66. A. Pais and S. B. Frieman, Phys. Rev. D $\underline{15}$, 2529 (1977).

67. W. Bacino et al., Stanford Linear Accelerator Center Report No. SLAC-PUB-2500 (1980), submitted for publication to Phys. Rev. Lett.

68. D. Fakirov and B. Stech, Nucl. Phys. $\underline{B133}$, 315 (1978).

69. This number is consistent with various determinations by different experiments. See Ref. 59 for details.

70. J. Prentice, to be published in the Proceedings of the VI International Conference on Experimental Meson Spectroscopy, Brookhaven National Laboratory, Upton, New York, April 25-26, 1980.

71. See for instance, M. L. Perl, Stanford Linear Accelerator Center Report No. SLAC-PUB-2446 (1979), to be published in Ann. Rev. Nucl. Part. Sci., for a review.

72. Y.-S. Tsai, Stanford Linear Accelerator Center Report No. SLAC-PUB-2450 (1979).

73. An observed photon with energy less than 100 MeV is likely to be a spurious signal caused by noise in the LA electronics.

74. G. S. Abrams et al., Phys. Rev. Lett. $\underline{43}$, 1555 (1979). A similar measurement by the DASP collaboration [R. Brandelik et al., Z. Phys. C $\underline{1}$, 233 (1979)] finds $B(\tau \to \rho \nu_\tau) = 24 \pm 9\%$.

75. This value of $\sin^2 \theta_c$ is obtained from the $K \to \mu \nu$ and $\pi \to \mu \nu$ partial decay widths, with no corrections made for the different K and π form factors. Hence, this value of $\sin^2 \theta_c$ is expected to be applicable to the K^* and ρ decay modes without correction for form factor differences.

76. This does not mean that none exist. Neither the masses nor the widths are well defined theoretically, and the decay modes expected for such states are often such that their detection by the Mark II would be difficult. For a brief but excellent review of the possibilities, see J. D. Bjorken, Stanford Linear Accelerator Center Report No. SLAC-PUB-2366, to be published in the Proceedings of the 1979 EPS High Energy Physics Conference, Geneva, Switzerland, June 27-July 4, 1979.